NYO 2243

Carnegie Institute of Technology

*Department of Physics*

# MEASUREMENT OF THE "ISOTOPE EFFECT" IN THE NUCLEAR CAPTURE OF NEGATIVE MUONS BY CHLORINE AND INVESTIGATION OF THE VALIDITY OF THE FERMI-TELLER "Z-LAW" IN AgCl

by

Walter J. Bertram, Jr.

Contract AT(30-1)-882

September, 1960

NYO-2243

# MEASUREMENT OF THE "ISOTOPE EFFECT" IN THE NUCLEAR CAPTURE OF NEGATIVE MUONS BY CHLORINE AND INVESTIGATION OF THE VALIDITY OF THE FERMI-TELLER "Z-LAW" IN AgCl

by

Walter J. Bertram, Jr.

September, 1960

Carnegie Institute of Technology

Contract AT(30-1)-882

A thesis, based upon the work reported here, has been submitted to the Department of Physics, Carnegie Institute of Technology, in partial fullfillment of the requirements for the degree of Doctor of Philosophy.

TABLE OF CONTENTS

LIST OF ILLUSTRATIONS

LIST OF TABLES

## ABSTRACT

Negative mu-mesons from the Carnegie Institute of Technology Synchrocyclotron have been used to study some of the interactions of these particles in various materials. Information concerning the interactions has been obtained by an analysis of the time distribution of the electrons resulting from the decay of muons which have been brought to rest in the material under study. In particular, the "isotope effect" in the nuclear capture of negative muons has been studied in separated isotopes of chlorine. The results are that the ratio of the capture rates in the two stable isotopes is $\lambda_c(Cl^{37})/\lambda_c(Cl^{35}) = 0.694 \pm 0.034$ . This is an even larger effect than predicted by the general theory of Primakoff, which gives 0.782 for this ratio. Unfortunately, no specific calculations for this effect in chlorine are available. Studies have also been made of the validity of the Fermi-Teller "Z-law", which predicts the probability of a negative meson becoming bound to a particular atomic species when the mesons are brought to rest in a chemical compound. These studies indicate that in AgCl, the muons are captured in equal numbers by the Ag and Cl atoms and not in the proportions predicted by the "Z-law". As a by-product of these investigations, the lifetimes of negative muons have been measured in Ag, Cl, and F. The results are $\tau_{Ag} = (91.5 \pm 2.3)$ nsec., $\tau_{Cl} = (0.437 \pm .022)$ μsec., and $\tau_F = (1.217 \pm .080)$ μsec.

# I. INTRODUCTION

In 1936, during investigations of the energy loss of cosmic ray electrons, it was noted that the observed data showed a difference in character among those particles[1,2,3,4]. Anderson and Neddermeyer[5] hypothesized the existence of particles of unit charge, but with a mass larger than that of an electron and much smaller than that of a proton. In 1937 Street and Stevenson[6] reported the detection in a cloud chamber of a particle with a mass approximately 130 times that of the electron. Neddermeyer and Anderson[7] later reported a value for the mass of this particle as 240 $m_e$, where $m_e$ is the mass of the electron.

This particle was at first identified as being the barytron predicted by Yukawa's theory of nuclear forces[8]. However, measurements by Johnson and Pomerantz[9] showed that the observed particle had a lifetime of $2.5 \times 10^{-6}$ sec., and Nordheim[10] showed that the Yukawa particle should have a lifetime much shorter than this.

During the period from 1939 to 1947, further effort was made to identify the meson, as the particle had come to be called, with the Yukawa barytron. In 1947, Conversi, Pancini, and Piccioni[11] studied the absorption of separated positive and negative mesons in iron and carbon. They showed that the capture rate of negative mesons was approximately $10^{12}$ times less than the expected value for the Yukawa particle[12]. Marshak and Bethe[13] then proposed the existence of a heavy meson which interacts strongly with nuclei (i.e., the Yukawa particle) and which can decay into the light or normal mesons observed in cosmic rays. This theory was supported by the data available from cosmic ray studies[14, 15] and the heavy and light mesons came to be known as the $\pi$ and $\mu$ mesons respectively.

With the discovery of the π-meson and its identification as the particle necessary for an understanding of nuclear forces, the μ-meson was relegated to the position of being merely a heavy electron, a particle for which there seemed to be no need in nuclear physics. The physical properties of the μ-meson may be summarized as follows:

Mass: $(206.76 \pm .03)m_e$ Charge: $\pm e$

Free Lifetime: $(2.211 \pm .003)$ μsec Spin: 1/2

Decay Process: $\mu^{\pm} \rightarrow e^{\pm} + \nu + \bar{\nu}$

Gyromagnetic Ratio: $2(1.00113 \pm .00016)$

Quantumelectrodynamical Value for

Spin 1/2 Particle: $2(1.00116)$ .

The hypothesis, in 1957, by Lee and Yang[17] of the violation in weak-interactions of the principle of conservation of parity led to renewed interest in the μ-meson. It was quickly shown[18,19] that the decay chain $\pi \rightarrow \mu \rightarrow e$ provided ample proof of the violation of the parity principle.

Following the overthrow of the parity principle, interest arose again over the possibility of a Universal Fermi Interaction involving the processes of β-decay, μ-decay, and μ-capture. It had been known for some time that the coupling constants in these processes were all of the same order of magnitude[20]. In the work of Feynman and Gell-Mann[21] on a Universal Fermi Interaction, it was shown that a universal coupling probably existed for β-decay and μ-decay. At that time, little was known of the details of the μ-capture interaction.

The disappearance reaction is most easily understood in terms of a process of the type $P + \mu \rightarrow N + \nu$ where the ν represents a neutrino[30]. The transition probability between a proton in state m and a neutron in

state j is

$$\lambda = (2\pi/\hbar)|M_{mj}|^2 \rho_f ,$$

where $\rho_f$ is the density of final states and $M_{mj}$ the matrix element for this transition. $M_{mj}$ is of the form

$$M = \sum_i g_i \int (\phi_n^* C_i \phi_p)(\phi_\nu^* C_i \phi_\mu) dV ,$$

where $C_i$ is a Dirac operator, $g_i$ is the appropriate coupling constant, and n, p, $\nu$, $\mu$, refer to neutron, proton, neutrino, and muon, respectively.

From measurements of the electron-neutrino correlation in β-decay, the β-decay interaction has been determined to be "V -A" . In the β-decay of the neutron, the ratio of the coupling constants was determined to be $g_A = -(1.21 \pm .03) g_V$. $g_A$ and $g_V$ are not equal because of virtual pion effects. If the Universal Fermi Interaction does exist, then the μ-capture reaction would also be of the form "V - A" . It has been pointed out[32,33] that in μ-capture there should also be an "induced" pseudoscalar interaction, although in the non-relativistic limit the direct pseudoscalar interaction is zero. The interaction arises from processes such as the one shown in the following diagram. The $\pi^+$ is a virtual pion, and the N,$\bar{N}$ represents a virtual nucleon-antinucleon pair.

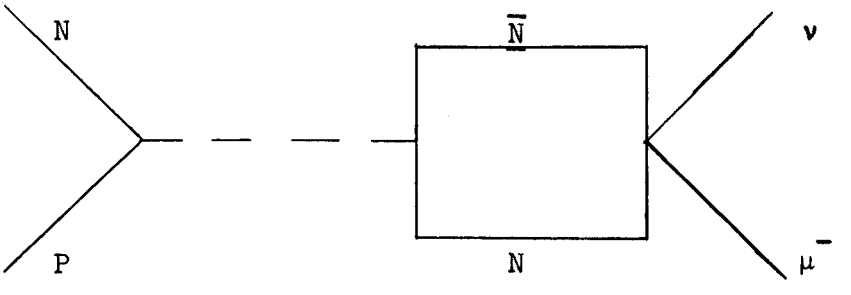


Goldberger and Treiman[32], using dispersion theory techniques to take account of the reaction $P \leftrightarrow N + \pi^+$ , showed that a "V - A" interaction

becomes a "(V + (weak magnetism)) - (A + cP)" interaction. Detailed calculations of the effects of virtual pions give the following results:[25]

1) $g_P^{(\mu)} = 8 g_A^{(\beta)}$

where $g_A^{(\beta)}$ is the value of $g_A$ measured in β-decay.

2) $g_V^{(\mu)} = .97\ g_V^{(\beta)}$

$g_M^{(\mu)} = 3.7\ g_V^{(\mu)}$

where $g_M$ is the value of the coupling constant due to the weak magnetism term.

3) $g_A^{(\mu)} = g_A^{(\beta)}$

The total capture rate depends almost entirely upon the magnitude and sign of an effective Fermi and an effective Gamow-Teller coupling constant:

$$G_F = g_V^{(\mu)}$$

$$G_T = g_A^{(\mu)} - \frac{\nu}{6M} \left( g_P^{(\mu)} + 2(g_M^{(\mu)} + g_V^{(\mu)}) \right),$$

where ν is the neutrino momentum.

The purpose of the work in measuring muon capture rates is to

1) Test the validity of a Universal Fermi Interaction

2) To detect the virtual pion effects.

The interpretation of measured muon capture rates is complicated by the fact that such measurements must, at the present time, be made on complex nuclei. The calculated capture rates are effected not only by the assumptions made about the interaction between muons and nucleons, but also by the particular model chosen to describe the nucleus.

Wheeler[22] calculated the capture rates of μ-mesons by nuclei using phenomenological arguments which are independent of the interaction mechanism. He assumed that the probability of absorption increases directly with the number of protons, and that the probability for

absorption by a single proton was proportional to the probability, $|\phi|^2$, for the meson to be in the neighborhood of this proton. The probability per second for absorption is

$$\lambda_c = \text{constant} \times \sum_{\substack{\text{all} \\ \text{protons}}} |\phi \text{ (at each proton)}|^2 .$$

For light nuclei, he used hydrogenic wave functions and found that

$$\lambda_c = \text{constant} \times (Z/\pi)(Ze^2\mu/\hbar^2)^3 ,$$

where $\mu$ is the meson mass. The constant has the dimensions of a volume, and is taken to be

$$\text{constant} = (1/t_o)(\hbar/\mu e^2)^3 (\pi/Z_o^4) ,$$

where $t_o$ is the natural mean life of the meson and $Z_o$ is a pure number. Then

$$\lambda_c = (1/t_o)(Z/Z_o)^4 .$$

For heavy nuclei, the hydrogenic approximation is not justified, and the capture rate is proportional to $\int |\phi(\vec{r})|^2 \rho(\vec{r}) d\vec{r}$, where $\rho$ is the density function of protons in the nucleus. $\phi(r)$ is the muon wave function normalized such that $\int |\phi|^2 d\vec{r} = \pi a_o^3$. The density function is normalized such that $\int \rho \, d\vec{r} = Z$. Wheeler found that the capture rate could be expressed as

$$\lambda_c = (1/t_o)(Z_{eff}/Z_o)^4 ,$$

where

$$(Z_{eff})^4 = \int |\phi(\vec{r})|^2 \rho(\vec{r}) d\vec{r} .$$

He evaluated this expression using approximate solutions of the Dirac equation for the muon wave function and assuming a uniform nuclear charge distribution, obtaining the following formula for $Z_{eff}$,

$$Z_{eff} = Z(1 + (Z/37.2)^{1.54})^{-1/1.54} .$$

The measurements of the capture rates[23] agreed with Wheeler's $(Z_{eff})^4$ law for the light elements up to Cu . For the heavier elements, the observed capture rates were much smaller than predicted by Wheeler.

A qualitative understanding of the deficiencies of Wheeler's theory can be gained by considering the kinematics of the decay process. A free nucleon at rest takes up about 5.5 Mev kinetic energy from the annihilation of the meson, while the remainder is carried off by the neutrino. A nucleon with 25 Mev kinetic energy cannot acquire more than about 22 Mev, while the neutrino will take off at least 85 Mev . If we consider the shell theory of the nucleus, in the ground state all of the lowest energy levels for protons and neutrons are occupied. If now, one of the protons becomes a neutron, because of the Pauli exclusion principle the neutron must be in one of the previously empty neutron levels, or else be ejected from the nucleus into an unbound state. In the heavier nuclei, where there is an excess of neutrons over protons, the effects of the Pauli exclusion principle become more pronounced, and the result is a capture rate less than that predicted by Wheeler's theory.

Various authors have improved upon the calculation of capture rates by considering the total absorption probability as the sum of contributions from individual particle transitions, in which a proton in some initial state is transformed into a neutron which must be in a state which was previously unoccupied.

Tolhoek and Luyten[26] have evaluated the ratio of the capture rates in Ni, Fe, Mn, Cr, V and Ti to the capture rate in Ca using shell model wave functions to evaluate the matrix elements. A potential well of infinite depth and of radius equal to $r_o A^{1/3}$ , where A is the atomic weight of the nucleus, was used. This is the radius of the well, and

not the radius of the matter distribution. The latter is considerably smaller than the radius of the well. In order to see the effect of the radius on the capture rate, two values of $r_o$ were used, $r_o = 1.40 \times 10^{-13}$ cm. and $r_o = 1.15 \times 10^{-13}$ cm. It is expected that the larger radius will correspond to a matter distribution which is closer to reality.

Sens[28] has measured these ratios and finds reasonable agreement with the theory if one uses equal amounts of Fermi and Gamow-Teller interaction and also adopts the "small" radius. The pure Fermi interaction, with "large" radius, cannot, however, be excluded. Quaranto[29] has measured the ratio of Fe/Ca and finds agreement with the Gamow-Teller interaction and the "small" radius, although the mixture of equal amounts of Fermi and Gamow-Teller interaction with "small" radius cannot be excluded. These results are not very conclusive as to the type of interaction involved in the $\mu$-capture process.

Primakoff[31] has made extensive calculations of the total muon capture rate using a closure approximation. The interaction hamiltonian used incorporates both the principles of non-conservation of parity and the assumption of a Universal Fermi Interaction. The interaction is taken to be of the form "V - A" and neutrinos are assumed to be emitted with unit negative helicity. An "induced" pseudoscalar interaction is also included. The calculation is quite complex, but straightforward. The transition probability from a proton in an initial state, a, to a neutron in the final state, b, is calculated using the assumptions indicated above. This transition probability involves the sum over all energetically accessible final states of the product of the square of the matrix element and a kinematic function of the neutrino momentum. Both of these quantities depend upon the final state, b. The closure

approximation extends the sum over all energetically accessible states b to a sum over all states b without restriction, and replaces the explicitly $E_b$-dependent quantities by suitable averages which do not depend upon $E_b$. The result of such a calculation gives

$$\lambda_c(a) = (Z_{eff})^4(\langle\eta\rangle_a)^2(272\ \text{sec}^{-1})R(1-I_a) .$$

$\langle\eta\rangle_a$ is the kinematical factor averaged over the final states. $272\ \text{sec}^{-1}$ is the value of the quantity

$$\frac{(m_\mu/m_e)^5}{(137)^3}\ \frac{\pi\ \ln 2}{(ft_{1/2})_{\text{neutron}}} .$$

R is the ratio of the assumed $\mu$-capture coupling constants to the coupling constant for the $\beta$-decay of the neutron. The quantity $I_a$ ($I_a > 0$) describes the inhibitory effect of the Pauli exclusion principle on the $\mu$-capture process. This is the inhibition arising from the fact that the resultant neutron cannot be produced in occupied states of the parent nucleus. $I_a$ may be expressed in terms of appropriate nucleon-nucleon correlation functions in the parent nucleus. Primakoff obtains $I_a = \frac{(A-Z)}{2A}\delta_a$ . $\delta_a$ is a "nucleon-nucleon correlation parameter", and is estimated from the experimental values of the Coulomb energy difference of various nuclei. The estimated value is $\delta_a = 3.0$ . Thus, the effect of the Pauli exclusion principle is proportional to the fraction of nucleons which are neutrons.

Sens[28] has made a least squares fit of his data to Primakoff's formula for the capture rate. He finds reasonable agreement, although there are some elements for which the disagreement is quite significant. This is to be expected because this theory should only predict the general trend of the capture rate as a function of Z and A, and not give

an exact value for any given nucleus. The values of the parameters obtained by Sens are:

$$\delta_a = 3.15 \; ; \qquad (\langle\eta\rangle_a)^2(272 \text{ sec}^{-1})R = 188 \text{ sec}^{-1} .$$

The expected value for $(\langle\eta\rangle_a)^2(272 \text{ sec}^{-1})R$ is 161 $\text{sec}^{-1}$ . Thus, one finds support for the assumptions on which the theory rests, viz.: a) that a "universal" interaction exists, and b) that two-component neutrinos are involved in $\mu$-capture, i.e., parity is not conserved. The agreement between theory and experiment involves only the strength of the coupling, and does not supply any information about the detailed structure of the interaction, e.g., the ratio between the Gamow-Teller and the Fermi interactions.

The theory of Tolhoek and Luyten[26] can, as we have seen, provide information on the structure of the interaction. They have also calculated the ratio of the capture rates in $Ca^{44}$ and $Ca^{40}$. The ratio for these two isotopes turns out to be independent of the type of interaction. A measurement of this ratio would provide a test of the nuclear part of the theory, i.e., determine the proper value of $r_o$ , and could eliminate the uncertainty in the comparison of theory to experiment.

In many experiments involving negative mesons, it is necessary to bring the mesons to rest in a chemical compound, e.g., bubble chamber liquids or nuclear emulsions. The interpretation of these experiments often requires knowing the relative probability of a meson being captured by the different kinds of atoms. In their paper on the capture of negative mesons in matter, Fermi and Teller[34] made the prediction that this capture probability is proportional to the nuclear charge, Z. They assumed that the capture probability was proportional to the energy loss of the meson in the vicinity of a given atomic species. On the basis of an expression

for the rate of energy loss by mesons in metals, they arrived at the prediction which has since come to be known as the "Z-law". The authors themselves considered the estimates made by them as crude, and pointed out that they are only reliable for metals. The case of insulators differs from that of metals because the amount of energy that may be delivered to electrons in a metal can be arbitrarily small, whereas in an insulator it must be at least as large as the gap between two Brillouin zones. The loss of energy to electrons will be thereby reduced in those cases in which energy is transferred in small individual amounts. In hydrogenous compounds, if the meson is captured on a hydrogen atom, the neutral mesonic atom may readily permeate to any part of the lattice. As a result, the meson may be caught in the field of a more highly charged nucleus.

Several groups of workers have made measurements testing the validity of the "Z-law"[35,36,37,38,39]. Two measurements[38,39] were made on hydrogenous materials and do not test the "Z-law" hypothesis. The calibration method used in reference 37 has been questioned[35]. Of the remaining work, except in the case of the metallic compound AgZn[36], it was found that the "Z-law" was not obeyed. In the work on AgZn it was found that, within the limits of the experimental error, the Z-law was obeyed.

Because of the importance of the "Z-law" to the interpretation of experimental data, it would be very desirable to further investigate the validity of this law in insulating materials, as well as in some more metallic compounds.

# II. EXPERIMENTAL METHOD

## A. GENERAL METHOD

The high intensity negative mu-meson beams available from present synchro-cyclotrons, along with the present day fast pulse and computer techniques, make the measurement of microsecond lifetimes possible with a hitherto unthought of accuracy. The measurement of the $\mu^+$ lifetime to an accuracy of approximately .13 percent is an example of the precision attainable[40]. The measurement of the lifetimes of the $\mu^-$ - meson in condensed materials is somewhat more difficult because the lifetime is shorter, and also because a significant number of the mesons may be captured by the nucleus before they can decay. For example, in silver, only 4 percent of the stopped muons decay, the rest are captured by the nucleus. This element has a meanlife which, in the present apparatus, corresponds to 1 channel, or 1/10 microsec.

In these experiments, we study the time distribution of the appearance of decay electrons from muons which stop in some target material. It will be shown below that such a distribution consists of a sum of exponential terms, and that the disappearance rate for each term is related to the rate at which mu-mesons are captured by a certain type of nucleus. Also, the relative amplitude of each exponential term is related to the relative number of muons which are bound in the K-orbit of each type of atom.

If a beam of negative mu-mesons is brought to rest in a suitable target material, $N_o(Z)$ of these will be captured by atoms with atomic number Z. Fermi and Teller[34] have shown that the time required for a muon to slow down from 2 kev and become bound in the K-orbit of an atom is of the order of $10^{-13}$ sec. This is much less than the lifetimes

we are considering here, and we may assume that the time at which the muon reaches the K-orbit is the same as the time that it entered the target. At time t=0 we have $N_o(Z)$ muons bound to atoms of atomic number Z. The rate at which muons disappear from the K-orbit is proportional to the number of muons present, and to the sum of the decay rates and capture rates. Thus,

$$dN/dt = -\left\{\lambda_d(Z) + \lambda_c(Z)\right\} N(t) ,$$

or

$$N(t) = N_o(Z) \exp\left\{-\lambda_t(Z)t\right\} ,$$

where $\lambda_t = \lambda_d + \lambda_c$ . The number of muons that decay at any time, t, is proportional to the number present and to the decay constant. The observed time spectrum, y(t), of electrons arising from muons bound to atoms of atomic number Z is proportional to the number that decay at any time, t, and to the detection efficiency, E, of the counter telescope. Thus,

$$y(t) = E\ dN_d/dt = E\ \lambda_d(Z)N_o(Z) \exp\left\{-\lambda_t(Z)t\right\} .$$

Now, in the time measuring apparatus used, we count the number of pulses from an oscillator which occur during the time interval to be measured. If T is the period of the oscillator, we use units of time where T=1 . If the time interval is of length nT + x , then the number of pulses counted can be either n or n + 1 , depending upon the

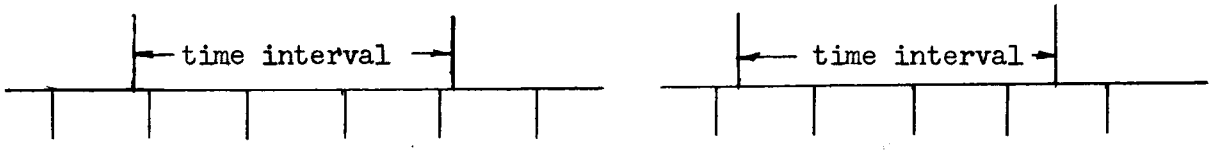


Time Interval = 3T + 1/4

relative phase between the beginning of the interval and the oscillator

pulses. This measuring system also has the effect of transforming the continuous decay spectrum into a histogram. The grouping of the spectrum into a histogram may be taken into account in the following manner. Let P(t) be the distribution of time intervals of length t. If the phase of the clock pulses were synchronized with the beginning of the time interval, then the histogram would be of the form

$$y_n = \int_n^{n+1} P(t)dt \ .$$

However, if there is a phase difference, $\phi$ $(0 \leqslant \phi < 1)$, between the clock pulse and the beginning of the time interval, the histogram will be of the form

$$y_n(\phi) = \int_{n-\phi}^{n+1-\phi} P(t)dt \ .$$

This is illustrated in the diagram.

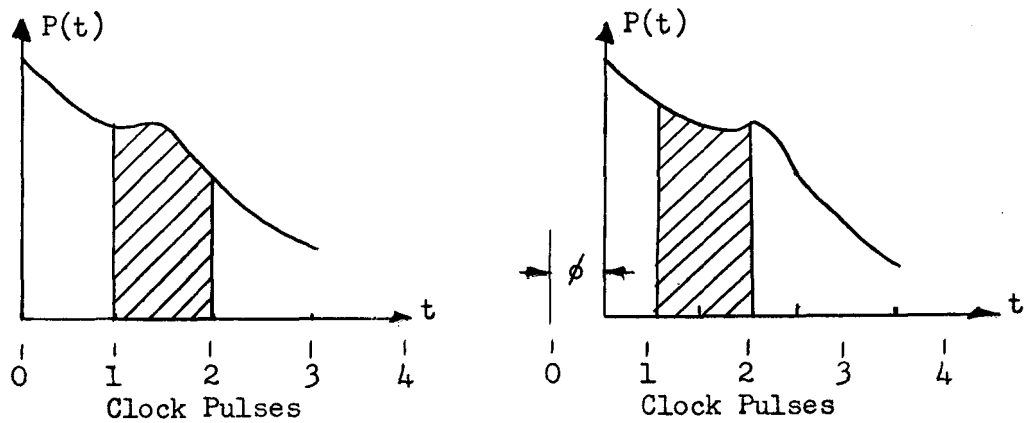


$y_1(0)$ would be the shaded area shown in the diagram to the left. If there were a phase $\phi \neq 0$, then $y_1(\phi)$ would be the shaded area shown in the diagram to the right and is seen to be the integral in the above equation. Since all values of $\phi$ between 0 and 1 are equally probable, the observed curve is obtained by averaging $y_n(\phi)$ over all values of $\phi$, i.e.,

$$\bar{y}_n = \int_0^1 y_n(\phi)d\phi \ .$$

We may illustrate this by considering a distribution of time intervals which all have the same length, N+x , corresponding to $P(t) = \delta(t-(N+x))$ , where $\delta(t)$ is the Dirac delta function. We then obtain

$$y_n(\phi) = \int_{n-\phi}^{n+1-\phi} P(t)dt = \begin{cases} 1 & ; \ -x < \phi < 1-x \ , \ n=N \\ 1 & ; \ 1-x < \phi < 2-x \ , \ n=N+1 \\ 0 & , \text{ all other values of } \phi \text{ and } n \ . \end{cases}$$

We may calculate $\bar{y}_n$, and find that

$$\bar{y}_n = \int_0^1 y_n(\phi)d\phi = \begin{cases} 1-x & , \ n=N \\ x & , \ n=N+1 \end{cases} \ .$$

This is interpreted as follows, if we make many measurements of the time interval of length N+x , a fraction (1-x) of the measurements will give N pulses, and a fraction (x) of the measurements will give N+1 pulses. The same result may be obtained by less sophisticated methods.

If we take for P(t) the time spectrum of electrons obtained before, $y(t) = E\lambda_d(Z)N_o(Z) \exp(-\lambda_t(Z)t) = Ke^{-\lambda t}$ ,

$$\text{then } y_n(\phi) = \int_{n-\phi}^{n+1-\phi} Ke^{-\lambda t}dt = K\frac{1-e^{-\lambda}}{\lambda} e^{-n\lambda} e^{\phi\lambda} \ ,$$

$$\text{and } \bar{y}_n = \int_0^1 y_n(\phi)d\phi = \frac{(1-e^{-\lambda})(e^{\lambda}-1)}{\lambda^2} Ke^{-n\lambda}$$

$$= F(\lambda)E\lambda_d(Z)N_o(Z) \exp(-n\lambda_t(Z)) \ .$$

The factor $F(\lambda)$ is given by

$$F(\lambda) = \frac{(1-e^{-\lambda})(e^{\lambda}-1)}{\lambda^2} = \frac{2}{\lambda^2}(\cosh\lambda - 1) \ .$$

$F(\lambda)$ may be expanded in powers of $\lambda$, and is found to be

$$F(\lambda) = 1 + \frac{1}{12}\lambda^2 + \frac{1}{360}\lambda^4 + \ldots$$

A plot of $F(\lambda)$ versus $\lambda$ is shown in Figure 8.

The effect of background counts in the electron counter telescope upon the form of the experimental curves must now be considered. These background counts arise from the random counting rate in the telescope due to neutrons and gamma-rays from the cyclotron. Consider first the following situation. If $S(t)$ is the probability of having no counts from time t=0 to time t, then $S(t+dt)$ is the probability of having no counts from time t=0 to time t+dt . The difference between these two quantities is the probability of having a count during the time interval dt . Hence, the probability per unit time of having the first count at time t is

$$\lim_{dt \to 0} \frac{S(t) - S(t+dt)}{dt} = - \frac{dS(t)}{dt} \quad .$$

We must now evaluate the quantity $S(t)$ . For random counts with the average rate R , the probability per unit time of having a count at time t is just R . If $S(t)$ is the probability of having no counts from time 0 to time t , then the probability of having the first count at time t is $S(t)R$ . This, however, is also given by $- dS/dt$ . Hence, we may equate these two quantities to form a differential equation for $S(t)$ ,

$$- \frac{dS}{dt} = S(t)R \quad .$$

This is easily integrated to give

$$S(t) = e^{-Rt} \quad ,$$

which is the probability of having no random counts during an interval of length t .

We must now consider the effect of the 20 microsec deadtime circuit in the electron telescope circuit (see Fig. 4). Since the maximum time interval which can be measured is 12 microsec, the deadtime circuit insures that there can only be one stop pulse during the 12 microsec interval in which a measurement may take place. Therefore, the probability of detecting a count from a decaying muon is just the product of the probability of such a count occurring, and the probability that there was no random count in the interval of length T=20 microsec before the count occurred. A random count in the 20 microsec interval before the muon decayed would have activated the deadtime circuit, preventing the detection of the count from the muon. If we denote by $\underline{a}$ , the probability per unit time of detecting a count from a muon, then

$$\underline{a} = e^{-RT} E\lambda_d e^{-\lambda t} .$$

The probability of detecting a random count will be the product of the probabilities of a random count occurring, the probability of no random counts occurring in the interval of length T before the random count occurred, and the probability that no count from a muon was detected in that interval. The probabilities are respectively R, $e^{-RT}$, and $1 - e^{-RT}\int_o^t E\lambda_d e^{-\lambda t} dt$ . If we denote by $\underline{b}$ , the probability per unit time of detecting a random count, then

$$\underline{b} = Re^{-RT}(1-e^{-RT}E\lambda_d/\lambda\ (1-e^{-\lambda t})) .$$

The probability of detecting either a muon count, a random count, or both simultaneously, in the interval of length dt will then be

$$y(t)dt = \underline{a}\ dt + \underline{b}dt - \underline{ab}\ (dt)^2 ,$$

and the observed decay curve will be the limit as $dt \to 0$ of $y(t)$,

which is just

$$y(t) = \underline{a} + \underline{b} = e^{-RT}\left\{E\lambda_d(1 + e^{-RT}R/\lambda)\ e^{-\lambda t} + R\ (1 - e^{-RT}E\lambda_d/\lambda)\right\} .$$

In these experiments, $R \leq 5 \times 10^{-4}$ per microsec, and $R/\lambda_t \ll 1$, $1 > e^{-RT} > 0.99$ . Therefore, to an accuracy sufficient for our purposes, the decay curve may be assumed to have the form

$$y(t) = E\lambda_d N_o(Z)\ e^{-\lambda_t(Z)t} + \text{constant} .$$

B. BEAM

A beam of mesons was obtained from the C.I.T. synchrocyclotron by allowing the internal proton beam to bombard a beryllium target. The fringing field of the cyclotron focusses mesons of different momenta into various channels in the shielding wall. A sector magnet was placed outside the shielding to improve the momentum selection and to remove neutral particles from the beam. The general arrangement used for obtaining the negative meson beam is shown in Figure 1.

The energy of the beam was determined to be $(43 \pm 3)$ Mev after passing through the first two monitor counters. A Cerenkov counter has been used to determine the electron contamination of the beam, and the beam was found to contain 30 percent electrons. The pi-meson contamination is less than 1/2 percent. The differential range curve of the beam is shown in Figure 5.

C. GEOMETRY

The experimental arrangement for the measurement of the capture rates in chlorine isotopes is illustrated in Figure 2. Counters 1 and 2 in coincidence and 3 in anti-coincidence indicate that a muon has stopped in the target. Counters 3 and 4 in coincidence and 2 or 5 in anti-coincidence indicate the detection of a decay electron. The aluminum absorber between counters 3 and 4 reduces the efficiency of

the electron telescope for detecting neutrons or gamma rays. Counters 2 and 5 , in anti-coincidence with the electron telescope, reduce the possibility of identifying beam associated particles as being decay electrons. This also prevents the detection of electrons from muons which decay immediately. This is taken into account by not including the first two channels in the analysis of the decay curves.

Although it is a standard practice to place a monitor counter directly in front of the target, it was found that such a counter greatly increased the carbon-background arising from muons which stop in the counters. Therefore, this counter was removed. The silver in front of the AgCl target was chosen so as to maximize the number of muons which stop in the target. Figure 6 shows the differential range curve of muons stopping in the $AgCl^{35}$ target. The Helmholtz coils were adjusted to buck out the fringing field of the cyclotron. This reduces the possibility of a sinusoidal modulation of the decay curve due to the precession of the muon spin about the field direction. The lead wall reduces the background rate in the electron telescope.

The experimental arrangement used for the test of the "Z-law" is shown in Figure 3. The aperture in the lead wall was enlarged to take advantage of the larger target available, and counter 5 was moved in front of the lead wall to accommodate the Cerenkov counter. The Cerenkov counter is connected in anti-coincidence with the counters 1 and 2 to prevent electrons from starting the clock mechanism. Figure 7 demonstrates the effect of the Cerenkov counter on the differential range curve.

D. COUNTERS

The scintillation counters were constructed using commercial plastic scintillant, optically coupled to lucite light pipes. The lightpipes were coupled to RCA 6810-A photomultiplier tubes. The tubes were operated according to the recommendations of the manufacturer, and were magnetically shielded from the fringing field of the cyclotron.

The Cerenkov counter was constructed of lucite, which acted both as a container for the radiator and as a light pipe. The radiator used was Fluorochemincal FC $75^{+}$ , which has an index of refraction of 1.276 . The minimum value of beta for which Cerenkov radiation can occur is $\beta = 0.784$ . The minimum energy at which radiation will occur is 67 Mev for muons; 320 kev for electrons; and 87 Mev for pions. The counter was viewed by two RCA 6810-A photomultiplier tubes, the outputs of which were added to form a single pulse. The counter had an efficiency of (101 $\pm$ 2) percent for counting the electron contamination of the beam, and was (99.4 $\pm$ 0.1) percent efficient when used as an anti-coincidence counter to discriminate against electrons in the beam.

E. ELECTRONICS

A block diagram of the electronic system is shown in Figure 4. The coincidence circuit, which is not shown, was modeled after the design given in UCRL Report 3307 Rev. A second muon which stops within 200 microsec. of the first one is prevented from interfering with the operation of the circuitry by the dead time circuit. The pulse forming circuit provides pulses of the proper shape to trigger the fast gate circuit, and also provides another pulse which is delayed by 15 microsec. This pulse is used to start the pulse height analyzer and also to close the

---

+ Minnesota Mining and Manufacturing Company

fast gate for those cases where no electron is detected. The fast gate produces a rectangular pulse with a rise (and fall) time of approximately $2 \times 10^{-9}$ sec. An rf signal is provided by a 10 Mc crystal controlled oscillator with a frequency of 10,001.6 kc. The variation of the frequency during the run was no greater than 0.1 kc. The rf signal from the oscillator, along with the pulse from the gate circuit, is fed into a coincidence circuit, the output of which is a pulse train whose length is the same as the length of the gate pulse. This pulse train is fed through a mixer circuit into a 10 Mc discriminator which shapes the pulse train, and then into a 10 Mc scaler. Fifteen microsec after the mu pulse, the delayed pulse from the pulse forming circuit initiates the storing process in the pulse height analyzer. First, a 2 Mc pulse train is fed to a scaler in the pulse height analyzer, and also through the discriminator and mixer into the 10 Mc scaler in which the 10 Mc pulse train has been stored. When the 10 Mc scaler counts up to 200, the overflow pulse is fed to the pulse height analyzer. This pulse stops the 2 Mc wave train and initiates the process in the analyzer which transfers the number from the internal scaler to the memory of the pulse height analyzer. The system is then ready to accept another muon pulse and start the analysis of the next time interval.

Two important characteristics of such a circuit are the linearity and the calibration. These two quantities have been measured in the following manner. The muon pulses are simulated by a pulse generator which has a large amount of jitter in the period of the pulses, and the electron pulses are simulated by pulses derived from the 10 Mc oscillator by scaling down by a factor of 500. The time interval, t, between a simulated muon pulse and the first following simulated electron

pulse has a distribution which is uniform for $0 < t < T$ , and there are no intervals with $t > T$ , where T is the period of the electron pulses. Furthermore, the number of counts, n, per channel is related to the total number of simulated muon pulses, N, and the scaling factor, S (S = 1/500), by the relation $n = SN$ . It should be noted that the two oscillators providing the mu and electron pulses must be isolated from one another, otherwise there will be a tendency for them to lock in phase, producing a distribution which is modulated by a sine wave.

The electronic system was checked by this method periodically during the time the data was being collected. The results of these check runs are presented in Table 1. The data from each check run was fitted, using the method of least squares, to a function of the form $n_i = n_o(1 + bi)$, where i is the channel number. The values of $X^2$ obtained were always consistent with the number of data points. The average value of b is less than the calculated standard deviation for this quantity, indicating that the system is linear to within $\pm$ 0.012 percent. $n_o$ also agrees with the quantity SN, indicating that the calibration is that one channel equals one 10 Mc oscillator period to within 0.06 percent. The only portion of the calibration data which displayed non-linearity was the first few channels, where the gate must be turned off shortly after it was turned on. This difficulty was overcome by inserting the 2 1/2 microsec delay in the electron pulse line. The channel corresponding to zero time delay between muon and electron pulses was channel 30 .

The linearity and calibration were also checked by using calibrated delay lines. These measurements showed the system to be linear to within 0.1 microsec, which is the limit of this method. The calibration obtained was again 0.1 microsec per channel.

TABLE 1

RESULTS OF LEAST SQUARES FIT TO CALIBRATION DATA

FITTED FUNCTION: $n_i = n_o(1 + bi)$

| Run No. | SN | $n_o$ | $b \times 10^4$ | $X^2$ |
|---|---|---|---|---|
| 256 | 28,826 | 28,799 ± 28 | (2.4 ± 2.8) | 107 |
| 269 | 15,327 | 15,346 ± 20 | -(2.8 ± 4.0) | 102 |
| 274 | 41,252 | 41,322 ± 40 | -(2.6 ± 2.8) | 135 |
| 289 | 12,501 | 12,553 ± 18 | -(5.2 ± 4.2) | 91 |
| 301 | 12,267 | 12,270 ± 24 | -(2.2 ± 6.0) | 154 |
| 331 | 15,892 | 15,902 ± 24 | (2.3 ± 4.4) | 132 |
| 342 | 19,577 | 19,586 ± 24 | (1.3 ± 3.8) | 93 |
| 343 | 13,544 | 13,559 ± 22 | -(0.2 ± 4.6) | 111 |
| 359 | 30,501 | 30,506 ± 32 | (3.0 ± 3.0) | 118 |
| 372 | 11,146 | 11,137 ± 18 | (5.0 ± 4.8) | 105 |
| 397 | 22,748 | 22,729 ± 28 | (5.1 ± 3.6) | 121 |
| Totals | 223,581 | 223,709 ± 84 | (.55 ± 1.22) | |

$$\frac{n_o - SN}{n_o} = 0.06 \text{ percent}$$

$\langle X^2 \rangle = 115 \pm 6$; Expected Value = 116

Standard Deviation of $X^2 = 19$

Expected Standard Deviation = 16

F. DATA ANALYSIS

The data recorded during the run was the number of muons stopped, the number of electron counts, the frequency of the 10 Mc oscillator, and the muon decay curve stored in the memory of the pulse height analyzer. The information on the time correlation between muons and electrons is a histogram of the form $y_n = \sum_i A_i e^{-n\lambda i}$ . One of the terms has $\lambda_i = 0$, i.e., the background term. One or more of the terms may have $\lambda_i$ equal to a known constant determined from other experiments. The carbon term is one of these, where $\lambda_t = (4.90 \times 10^5 \text{ sec}^{-1})^{40}$. The term arising from Ag, where AgCl is the target material, is another. The histograms were treated by the method of least squares to obtain the $A_i$ and any unknown $\lambda_i$ . The least squares analysis is discussed in Appendix A. The computation involved was performed using an IBM type 650 digital computer. The programming of this machine is discussed in Appendix B.

The data on the chlorine isotopes was obtained in the following manner. The two isotopes were alternately studied for periods of four hours apiece. In this manner, approximately 35 thousand chlorine decays from each target were observed. The data from each four hour period were added together and fitted to the function

$$y_n = A(\alpha_{35}\, e^{-n\lambda_t(35)} + \alpha_{37}\, e^{-n\lambda_t(37)}) + B\, e^{-n\lambda_t(Ag)} + C\, e^{-n\lambda_t(C)} + D \,.$$

The $\alpha$'s are the product of the factor $F(\lambda)$, discussed in Section II-A, and the isotopic concentrations in the target. For the $Cl^{35}$ target, the isotopic concentrations were 96.8 percent $Cl^{35}$ and 3.2 percent $Cl^{37}$ , for the $Cl^{37}$ target they were 76.0 percent $Cl^{37}$ and

24.0 percent $Cl^{35}$ . The analysis was made in the following manner. $\lambda_t(35)$ was calculated from the data on the $Cl^{35}$ target, using $\alpha_{37} = 0$ . Then, this value of $\lambda_t(35)=\lambda_t^{(1)}(35)$ , was used to calculate $\lambda_t^{(1)}(37)$ using the isotopic concentrations for the $\alpha$'s. Then $\lambda_t^{(2)}(35)$ was calculated using the isotopic concentrations for the $\alpha$'s and using $\lambda_t^{(1)}(37)$ . This process was repeated, alternately calculating $\lambda_t^{(i)}(35)$ and $\lambda_t^{(i)}(37)$ until the changes in the decay rates were negligible. Then the values of $F(\lambda)$ were calculated from the final values of the $\lambda_t$ . Using $\alpha=F(\lambda)$ x (isotopic concentration), the process was repeated. It was found that the inclusion of $F(\lambda)$ made a negligible difference in the calculated disappearance rates.

The data relating to the "Z-law" was analyzed in the following manner. The AgCl decay curve from a target composed of the natural isotopic mixtures of Ag and Cl was analyzed to determine the amplitudes of the Ag, Cl, C, and background components. From these amplitudes the quantities $EN_o(Z)$ may be obtained, and the ratio $R=EN_o(Cl)/EN_o(Ag)$ calculated. E is the efficiency of the electron telescope and is assumed to be the same for electrons from Ag and Cl. The method of calculating $N_o(Z)$ from the data is discussed in Section II-A . The values of $\lambda_d(Z)$ used in calculating $N_o(Z)$ are taken from the paper of Yovanovitch[41] .

# III. RESULTS

## A. RESULTS OF THE "ISOTOPE EFFECT" INVESTIGATION

The data from each of the chlorine targets were fitted to the histogram discussed in Section II-F. The results of these calculations are shown in the following table. The data, along with the fitted functions, are shown in Figure 9. This graph shows only the first six microseconds of the decay curves. The portion from 6 to 12 microsec consists mainly of the carbon component and the constant term. The standard deviation on each point (which is not shown for purposes of clarity) is equal to the square root of the number of counts in each channel.

Table 2

| Target | Amp. Cl | Amp. Ag | Amp. C. | Amp. Const. | $X^2$ | Expected $X^2$ |
|---|---|---|---|---|---|---|
| $Cl^{35}$ | 7057 ±350 | 10,206 ±5,000 | 763 ±30 | 267 ± 2 | 120 | 113 ± 15 |
| $Cl^{37}$ | 5995 ±240 | 14,052 ±6,800 | 690 ±35 | 219 ± 2 | 123 | 113 ± 15 |

$$\lambda_t(35) = (22.54 \pm .52) \times 10^5 \text{ sec}^{-1}$$

$$\lambda_t(37) = (17.03 \pm .49) \times 10^5 \text{ sec}^{-1}$$

The measurements of Yovanovitch[41] show that in the region of chlorine, $\lambda_d(Z)$ is the same as $\lambda_d(0)$, the decay constant of the free muon. Using the value of $4.52 \times 10^5$ sec$^{-1}$ for the decay constant of the free muon[40], we obtain the following values for the capture rates:

$$\lambda_c(35) = (18.02 \pm .52) \times 10^5 \text{ sec}^{-1}$$

$$\lambda_c(37) = (12.51 \pm .49) \times 10^5 \text{ sec}^{-1} \quad .$$

The ratio $\lambda_c(37)/\lambda_c(35)$ is $0.694 \pm 0.034$ , and the ratio of the difference in the capture rates to the mean value of the capture rate is

$$\frac{\lambda_c(35) - \lambda_c(37)}{\bar{\lambda}_c} = (36.1 \pm 4.6) \text{ percent} .$$

The only theoretical prediction which can be compared with the results of this experiment is the estimate of Primakoff[31] for the capture rates. If these data are fitted to the formula of Primakoff, $\lambda_c = (Z_{eff})^4(\langle\eta\rangle_a)^2(272 \text{ sec}^{-1})R(1- \delta_a \frac{A-Z}{2A})$ , we obtain

$$\delta_a = 3.3 \pm .06$$

$$(\langle\eta\rangle_a)^2(272 \text{ sec}^{-1})R = 303 \pm 36 \text{ sec}^{-1} .$$

The expected values are 3.0 and 161 $\text{sec}^{-1}$ respectively. This discrepancy is not serious, however, since we expect individual nuclei to have significant fluctuations from Primakoff's formula. In fact, since in going from $Cl^{35}$ to $Cl^{37}$, we close the neutron shell in which many of the capturing protons originally were located, we expect to have an exceptionally large exclusion principle effect.

## B. RESULTS OF THE "Z-LAW" INVESTIGATION

The results of the analysis performed on the data pertaining to the atomic capture of μ-mesons in AgCl is presented in Table 3.

Table 3

| | |
|---|---|
| Ag Amplitude: | $2430 \pm 330$ |
| Cl Amplitude: | $3010 \pm 250$ |

$$\frac{N_o(Cl)}{N_o(Ag)} = \frac{\text{Amp (Cl)}}{F(\lambda_t(Cl))\lambda_d(Cl)} \frac{F(\lambda_t(Ag))\lambda_d(Ag)}{\text{Amp (Ag)}} = 1.09 \pm .17$$

This result is in agreement with the results of Sens, et al.,[35] who found that the "Z-law" was not obeyed in insulating materials, but rather that the observed capture ratios follow more closely the simple atomic ratios, unweighted by the atomic numbers of the elements.

## C. CAPTURE RATES OF NEGATIVE MUONS IN VARIOUS MATERIALS

During the course of these investigations it has been necessary to measure the value of the disappearance rates of negative muons in various materials. These rates are listed in Table 4, along with the estimated values of the decay rates of negative muons in these materials and the values of the capture rates. The decay rates have been estimated using the values of $\lambda_d(Z)/\lambda_d(0)$ obtained by Yovanovitch[41] and the value of $\lambda_d(0)$ obtained by Reiter, et al.[40] For comparison, the values of the capture rates obtained by Swanson, et al.,[42] are also listed.

Table 4

| Material | Natural Silver | Natural Chlorine | Natural Florine |
|---|---|---|---|
| $\tau_{mean}(\mu sec)$ | .0915 ± .0023 | .437 ± .022 | 1.217 ± 0.080 |
| $\lambda_t(Z)$ | 109.2 ± 2.7 | 22.9 ± 1.1 | 8.22 ± .54 |
| $R = \frac{\lambda_d(Z)}{\lambda_d(0)}$ | 0.90 ± 0.05 | 1.00 ± 0.03 | 1.00 ± 0.02 |
| $\lambda_d(Z)$ | 4.07 | 4.52 | 4.52 |
| $\lambda_c(Z)$ | 105.1 ± 2.7 | 18.4 ± 1.1 | 3.70 ± 0.54 |
| $\lambda_c(Z)_{Swanson}$ | 112.5 ± 5.0 | 13.9 ± 0.9 | 2.54 ± 0.22 |

All rates are in units of $10^5$ $sec^{-1}$.

There is considerable disagreement between the values obtained for Cl and F. It should be noted that if the carbon background were not taken into account, the effect would be to decrease the disappearance rate, since what is being measured is an average between the carbon disappearance rate and the actual rate under investigation. This was illustrated by analyzing our data without making allowances for the carbon. The results are values of $\lambda_t(Cl)$ and $\lambda_t(F)$ which are much closer to the values obtained by Swanson, but the "goodness of fit" obtained is much poorer than that obtained when allowances are made for the carbon.

# APPENDIX A

## METHOD OF LEAST SQUARES FOR FITTING DATA TO A SUM OF EXPONENTIAL TERMS

The problem is to make a least squares fit to a function which is a sum of exponential terms, where both the amplitudes and the decay constants may be unknown. Since no exact solution of this problem is known, the following iterative procedure has been adopted. We wish to make a least squares fit to a function of the form $f_i = \sum_j \alpha_j g_{ij}$ , where the $\alpha_j$ are the amplitudes and $g_{ij} = e^{-i\lambda_j}$ . We expand the $g_{ij}$ as follows:

$$g_{ij}(\lambda_j) = g_{ij}(\bar{\lambda}_j) + \left(\frac{d}{d\lambda_j} g_{ij}(\lambda_j)\right)\Bigg|_{\lambda_j=\bar{\lambda}_j} (\lambda_j - \bar{\lambda}_j) + \ldots$$

If $\lambda_j - \bar{\lambda}_j \equiv \nu_j$ , then

$$\alpha_j e^{-i\lambda_j} \cong \alpha_j e^{-i\bar{\lambda}_j} - (\alpha_j \nu_j) i e^{-i\bar{\lambda}_j}$$

In this manner, the problem is reduced to a linear least squares fit, which is easily solved for the most probable values of the $\alpha_j$ and $(\alpha_j \nu_j)$ . From these results, we can compute $\nu_j = (\alpha_j \nu_j)/\alpha_j$ , which is the correction to the decay constant. We then replace $\bar{\lambda}_j$ by $\bar{\lambda}_j + \nu_j$ and perform the calculation again. This iterative process is repeated until the values of $\nu_j$ obtained are less than $10^{-4} \times \bar{\lambda}_j$ .

The problem of making a linear least squares fit to a sum of exponential terms is solved in the following manner. We let $y_i$ be the set of measured points, $\sigma_i$ the standard deviation of the value of $y_i$ , and $f_i = \sum_{j=1}^{J} \alpha_j g_{ij}$ the function to which we wish to make a fit. The quantity we wish to minimize is $X^2 = \sum_{i=1}^{N} (y_i - f_i)^2 / \sigma_i^2$ .

The distribution of the quantity $X^2$ has been studied extensively, and the following results may be stated[43]. The average value of $X^2$ (obtained from many sets of data) should be N-J-1 , where N is the number of data points included in the summation, and J is the number of parameters which are determined from the data. The standard deviation of a measurement of $X^2$ is $\text{s.d.}X^2 = \sqrt{2(N-J-1)}$ , provided that $(N-J-1) \geq 30$ .

The method of calculating the $\alpha_j$ proceeds as follows.

We set $\partial X^2 / \partial \alpha_j \equiv 0$ , $\quad j = 1,2,\ldots J$ .

The set of equations we obtain is

$$\sum_i \frac{\partial f_i}{\partial \alpha_j} (y_i - f_i)/\sigma_i^2 = 0 \quad , \qquad j = 1,2,\ldots J \qquad (1)$$

Since $\partial f_i / \partial \alpha_j \equiv g_{ij}$ , we may write equation (1) as

$$\sum_i \{g_{ij} y_i / \sigma_i^2\} - \sum_i \{g_{ij} f_i / \sigma_i^2\} = 0 \quad , \quad j = 1,2,\ldots J$$

or

$$\sum_i \{g_{im} y_i / \sigma_i^2\} - \sum_i \{g_{im} (\sum_j \alpha_j g_{ij}) / \sigma_i^2\} = 0 \ , \ m = 1,2,\ldots J$$

If we interchange the order of the summation, we obtain

$$\sum_j \{\alpha_j (\sum_i g_{im} g_{ij} / \sigma_i^2)\} = \sum_i \{g_{im} y_i / \sigma_i^2\}, \ m = 1,2,\ldots J \qquad (2)$$

We may define

$$G_{mj} \equiv \sum_i \{g_{im} g_{ij} / \sigma_i^2\} \ ; \ V_m \equiv \sum_i g_{im} y_i / \sigma_i^2 \ ,$$

then we can write equation (2) as a matrix equation,

$$\sum_j \alpha_j G_{mj} = V_m \ .$$

This equation is solved for the $\alpha_j$ by making use of the inverted matrix, $(G_{mj})^{-1}$, then

$$\alpha_j = \sum_m (G_{mj})^{-1} V_m \ .$$

For the case where the $y_i$ are distributed according to a Poisson distribution, $\sigma_i^2 = y_i$, and

$$G_{mj} = \sum_i g_{im} g_{ij} / y_i \quad ; \quad V_m = \sum_i g_{im} \ .$$

It is desirable to know the standard deviation of the $\alpha_j$ determined in this manner. The standard deviation may be written as follows:

$$\text{s.d.}\alpha_j = \sqrt{\frac{X^2}{N-J-1} \sum_i \left(\frac{\partial \alpha_j}{\partial y_i} \sigma_i\right)^2} \ .$$

The first factor gives the dependence of $\text{s.d.}\alpha_j$ on the variance, or goodness of fit, of the set of data. The second factor gives the $\text{s.d.}\alpha_j$ due to the dependence of $\alpha_j$ on the $y_i$, and the inherent standard deviation of the $y_i$. The second factor is calculated in the following manner.

$$\alpha_j = \sum_m (G_{mj})^{-1} V_m$$

$$\frac{\partial \alpha_j}{\partial y_i} = \sum_m \left(G_{mj}^{-1} \frac{\partial V_m}{\partial y_i} + \frac{\partial G_{mj}^{-1}}{\partial y_i} V_m\right)$$

$$= \sum_m G_{mj}^{-1} \, g_{im}/\sigma_i^2$$

$$\frac{\partial \alpha_j}{\partial y_i} \sigma_i = \sum_m G_{mj}^{-1} \, g_{im}/\sigma_i$$

$$\left(\frac{\partial \alpha_j}{\partial y_i}\,\sigma_i\right)^2 = \sum_m \sum_p \left(G_{mj}^{-1}\, g_{im}/\,\sigma_i\right)\left(G_{pj}^{-1}\, g_{ip}\,/\sigma_i\right)$$

$$= \sum_m \sum_p G_{mj}^{-1}\, G_{pj}^{-1}\, \left(g_{im} g_{ip}\,/\,\sigma_i^2\right)$$

$$\sum_i \left(\frac{\partial \alpha_j}{\partial y_i}\,\sigma_i\right)^2 = \sum_m \sum_p G_{mj}^{-1}\, G_{pj}^{-1}\, G_{mp}$$

$$= \sum_m G_{mj}^{-1}\, (1)_{mj}$$

$$= G_{jj}^{-1}$$

$(1)_{mj}$ is the diagonal matrix. We then see that

$$\text{s.d.}\alpha_j = \sqrt{\frac{X^2}{N-J-1}\, G_{jj}^{-1}}$$

The application of this method to the histogram obtained from the AgCl "isotope effect" data will be illustrated. The function to which we desire to fit the data is

$$f_n = A\left(a_{35}\, e^{-n\lambda(35)} + a_{37}\, e^{-n\lambda(37)}\right) + B\, e^{-n\lambda(Ag)} + C\, e^{-n\lambda(C)} + D\,.$$

If we expand $e^{-n\lambda(35)}$ as indicated above, we obtain

$$f_n = A\left(a_{35}\, e^{-n\bar{\lambda}(35)} + a_{37}\, e^{-n\lambda(37)}\right) + (A\nu)\left(-a_{35} n\, e^{-n\bar{\lambda}(35)}\right)$$

$$+ B\, e^{-n\lambda(Ag)} + C\, e^{-n\lambda(C)} + D\,.$$

The forms of the $\alpha_j$ and $g_{ij}$ to be used are:

$\alpha_1 = (A\nu)$ $\qquad$ $g_{n1} = -a_{35} n\, e^{-n\bar{\lambda}(35)}$

$\alpha_2 = A$ $\qquad$ $g_{n2} = a_{35}\, e^{-n\bar{\lambda}(35)} + a_{37}\, e^{-n\lambda(37)}$

$\alpha_3 = B$ $\qquad$ $g_{n3} = e^{-n\lambda(Ag)}$

$\alpha_4 = C$ $\qquad$ $g_{n4} = e^{-n\lambda(C)}$

$\alpha_5 = D$ $\qquad$ $g_{n5} = 1$

The method of calculating the $\alpha_j$ is discussed in Appendix B.

## APPENDIX B

## COMPUTER PROGRAMMING FOR THE DATA ANALYSIS

The calculations involved in making a least squares fit to a function containing four exponential terms and involving 150 data points are quite tedious and extremely lengthy. For these reasons, all of the computation was done on an IBM type 650 digital computer. The programming for this machine was done using the generalized algebraic translating system GATE, written by the staff of the Carnegie Computation Center. Because programs written for this system cannot be used directly with most other systems, and since the language involved is highly specialized, the programs, as such, are not described in this work. However, the general method used in the calculation of $\lambda(35)$ and $\lambda(37)$ is described with the aid of the appropriate flow charts. Figure 10a is the flow chart pertaining to the overall system of the calculations. Figure 10b is the flow chart pertaining only to the calculation of $\lambda$, $\nu$, and $\alpha_j$ with a given set of initial guesses for the $\lambda$ .

Figure 10a will be described first. The information read into the computer is the data, initial guesses for $\lambda_t(35)$ and $\lambda_t(37)$, values of $\lambda_t(Ag)$ and $\lambda_t(C)$, the convergence criterion C, and the first and last data points to be used in the calculation. I is a constant which tells the "compute" subroutine whether to use data from the $Cl^{35}$ or $Cl^{37}$ targets and which $\lambda$ it is to calculate, etc. The "compute" subroutine is described in the next paragraph. For a given initial guess for $\lambda$, "compute" will supply the $\nu$ and $\alpha_j$ . This process is repeated until $\nu/\lambda$ is less than the convergence criterion. After convergence of $\lambda(35)$ has been obtained, the results are stored and computation proceeds to $\lambda(37)$. When a final value of $\lambda(37)$ has been

obtained, the results are stored. Next, the program compares the computed values of $\lambda$ with the initial guesses. If there has been a large change in $\lambda$, the latest values of $\lambda$ are used as initial guesses and the process is repeated. When a final convergence has been obtained, the function $f_n$ , the residuals $v_n = y_n - f_n$ , and $X^2$ are calculated. Then the standard deviations of the $\lambda$ and the $\alpha_j$ are computed. Finally all the pertinent quantities are punched on cards and the calculation is complete.

The "compute" subroutine shown in Figure 10b proceeds as follows. For a given value of n , the matrix elements $G_{mj}$ and $V_m$ are computed, using the present value of $\underline{I}$ to decide as to which data, etc., are to be used. The inversion of the matrix $G_{mj}$ is accomplished by using a subroutine built into the GATE system. The values of the $\alpha_j$ and $\nu$ are then computed, and control proceeds according to the flow chart in Figure 10a.

## APPENDIX C

## EVALUATION OF THE EFFECT OF SECOND MU'S ON THE DECAY CURVES

Suppose that the instantaneous muon counting rate is $\lambda_\mu$. Then, if at a time t = 0 we stop a muon in the target, the distribution in time of second, or the next arriving, muon will be

$$P_\mu(t) = \lambda_\mu e^{-\lambda_\mu t} .$$

For a second muon which stops in the target at time t, the distribution of electron counts is

$$\bar{P}_e(t,t') = E\,\lambda_d\, e^{-\lambda_t(t'-t)} \quad , \quad t' \geqslant t \ ,$$

$$\bar{P}_e(t,t') = 0 \quad , \quad t' < t \ ,$$

where t' is the time at which the electron is emitted. The distribution in time of electrons emitted by second muons, where zero time is when the first muon stopped, is given by

$$P_e^{(2)}(t') = \int_o^{t'} \bar{P}_e(t,t')\, P_\mu(t)dt .$$

The integral is easily evaluated to give

$$P_e^{(2)}(t) = \frac{E\lambda_\mu\lambda_d}{\lambda_t-\lambda_\mu}\left(e^{-\lambda_\mu t} - e^{-\lambda_t t}\right) \ ,$$

where t' was replaced by t. The general features of this function are shown schematically in the following graph. In these experiments, $\lambda_\mu << \lambda_t$ , $\lambda_\mu t_{max} << 1$ , and the function may be approximated by

$$P_e^{(2)}(t) \cong \frac{E\lambda_\mu\lambda_d}{\lambda_t}\left(1 - e^{-\lambda_t t}\right) .$$

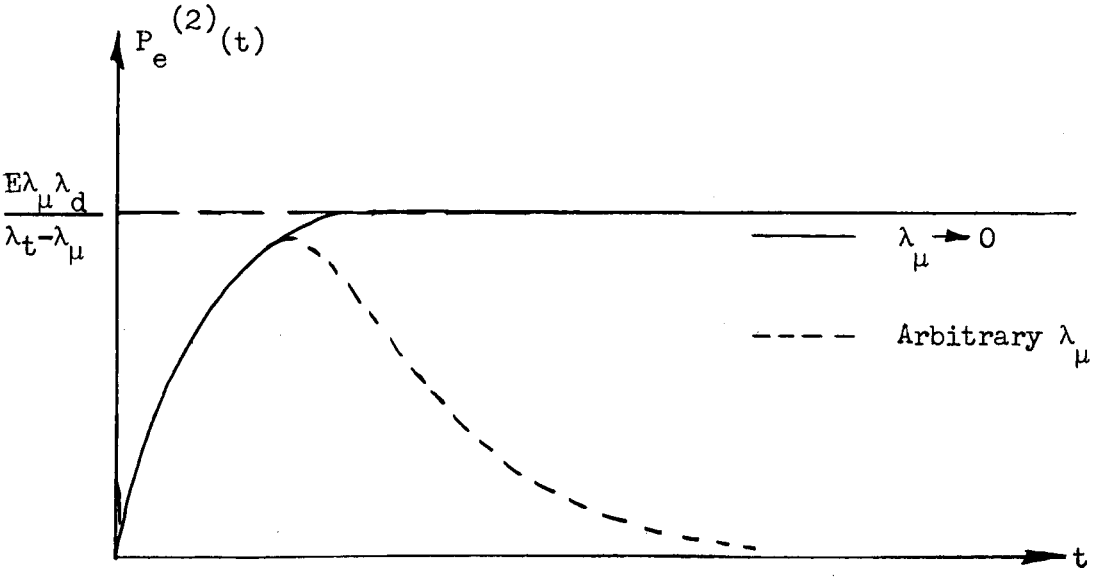


The interesting quantity is the ratio of the amplitude of $P_e^{(2)}(t)$ to the amplitude of the distribution function for electrons from the first muon, $P_e^{(1)}(t) = E\,\lambda_d\, e^{-\lambda_t t}$ . This quantity is given by

$$R = \frac{E\lambda_\mu\lambda_d/\lambda_t}{E\lambda_d} = \lambda_\mu/\lambda_t \quad .$$

For the chlorine "isotope effect" experiment, the value of R was $7 \times 10^{-5}$ , and the effects of the second muons are certainly negligible.

LIST OF REFERENCES


1. Crussord and Leprince-Ringuet, Compt. rend. 204, 240 (1937)
2. C. D. Anderson and S. H. Neddermeyer, Phys. Rev. 50, 263 (1936)
3. B. Rossi, Zeits. Physik, 82, 151 (1933)
4. J. C. Street, et al., Phys. Rev. 47, 891 (1935)
5. S. H. Neddermeyer and C. D. Anderson, Phys. Rev. 51, 884 (1937)
6. J. C. Street and E. C. Stevenson, Phys. Rev. 52, 1003 (1937)
7. S. H. Neddermeyer and C. D. Anderson, Phys. Rev. 54, 88 (1938)
8. H. Yukawa, Proc. Phys.-Math. Soc. Japan 17, 48 (1935)
9. T. H. Johnson and M. A. Pomerantz, Phys. Rev. 55, 104 (1939)
10. L. W. Nordheim, Phys. Rev. 55, 506 (1939)
11. M. Conversi, E. Pancini, and O. Piccioni, Phys. Rev. 71, 209 (1947)
12. E. Fermi, E. Teller and V. Weisskopf, Phys. Rev. 71, 314 (1947)
13. R. E. Marshak and H. A. Bethe, Phys. Rev. 72, 506 (1947)
14. Lattes, Muirhead, Occhialini, and Powell, Nature 159, 694 (1947)
15. G. F. Chew, Phys. Rev. 73, 1128 (1948)
16. J. R. Richardson, Phys. Rev. 74, 1720 (1948)
17. T. D. Lee and C. N. Yang, Elementary Particles and Weak Interactions BNL 443 (T-91)
18. R. L. Garwin, L. M. Lederman, and M. Weinrich, Phys. Rev. 105, 1415 (1957)
19. J. I. Friedman and V. L. Telegdi, Phys. Rev. 105, 1681 (1957)
20. See, e.g., E. Fermi, Elementary Particles, (Yale University Press, 1951)
21. R. P. Feynman and M. Gell-Mann, Phys. Rev. 109, 193 (1958)
22. J. A. Wheeler, Rev. Mod. Phys. 21, 133 (1949)
23. J. W. Keuffel, F. B. Harrison, T.N.K. Godfrey, G. T. Reynolds Phys. Rev. 87, 942 (1952)

24. M. G. Mayer and J. H. D. Jensen, Elementary Theory of Nuclear Shell Structure, (John Wiley and Sons, Inc., 1955)

25. L. Wolfenstein, Paper presented at the 1960 Rochester Conference

26. H. A. Tolhoek and J. R. Luyten, Nuclear Phys. 3, 679 (1957)

27. W. Pauli, Zeits. Physik 43, 601 (1927)

28. J. C. Sens, Phys. Rev. 113, 679 (1959)

29. A. A. Quaranto, et al., Il Nuova Cimento XIV, 48 (1959)

30. For a survey of the arguments, see R. D. Sard and M. F. Crouch, in Progress in Cosmic Ray Physics, edited by J. G. Wilson, (North-Holland Publishing Co., Amsterdam, 1954), Vol. 2

31. H. Primakoff, Rev. Mod. Phys. 31, 802 (1959)

32. M. L. Goldberger and S. B. Treiman, Phys. Pev. 111, 354 (1958)

33. L. W. Wolfenstein, Il Nuova Cimento 8, 882 (1958)

34. E. Fermi and E. Teller, Phys. Rev. 72, 399 (1947)

35. J. C. Sens, R. A. Swanson, V. L. Telegdi, D. D. Yovanovitch, Il Nuova Cimento 72, 399 (1947)

36. J. F. Lathrop, R. A. Lundy, R. A. Swanson, V. L. Telegdi, D. D. Yovanovitch, Il Nuova Cimento 15, 831 (1960)

37. M. B. Stearns and M. Stearns, Phys. Rev. 105, 1573 (1957)

38. A. Faformar and M. H. Shomos, Phys. Rev. 100, 874 (1955)

39. W. K. H. Panofsky, R. L. Aamodt, and J. Hadley, Phys. Rev. 81, 565 (1951)

40. R. A. Reiter, T. A. Romanowski, R. B. Sutton, and B. G. Chidley, Phys. Rev. Letters 5, 22 (1960)

41. D. D. Yovanovitch, Phys. Rev. 117, 1580 (1960)

42. R. A. Swanson, Phys. Rev. 112, 580 (1958)

43. H. Cramer, Mathematical Methods of Statistics (Princeton University Press, 1946)

ACKNOWLEDGEMENTS

The author wishes to express his thanks for the advice and help of Professer Roger Sutton and Dr. Thomas Romanowski. The help of Messrs. R. Reiter, M. Eckhouse, T. Filippas, E. Gray and J. Stachew is greatly appreciated. The Fellowship support of the National Science Foundation during the past four years was gratefully appreciated.

This work was partially supported by the United States Atomic Energy Commission.

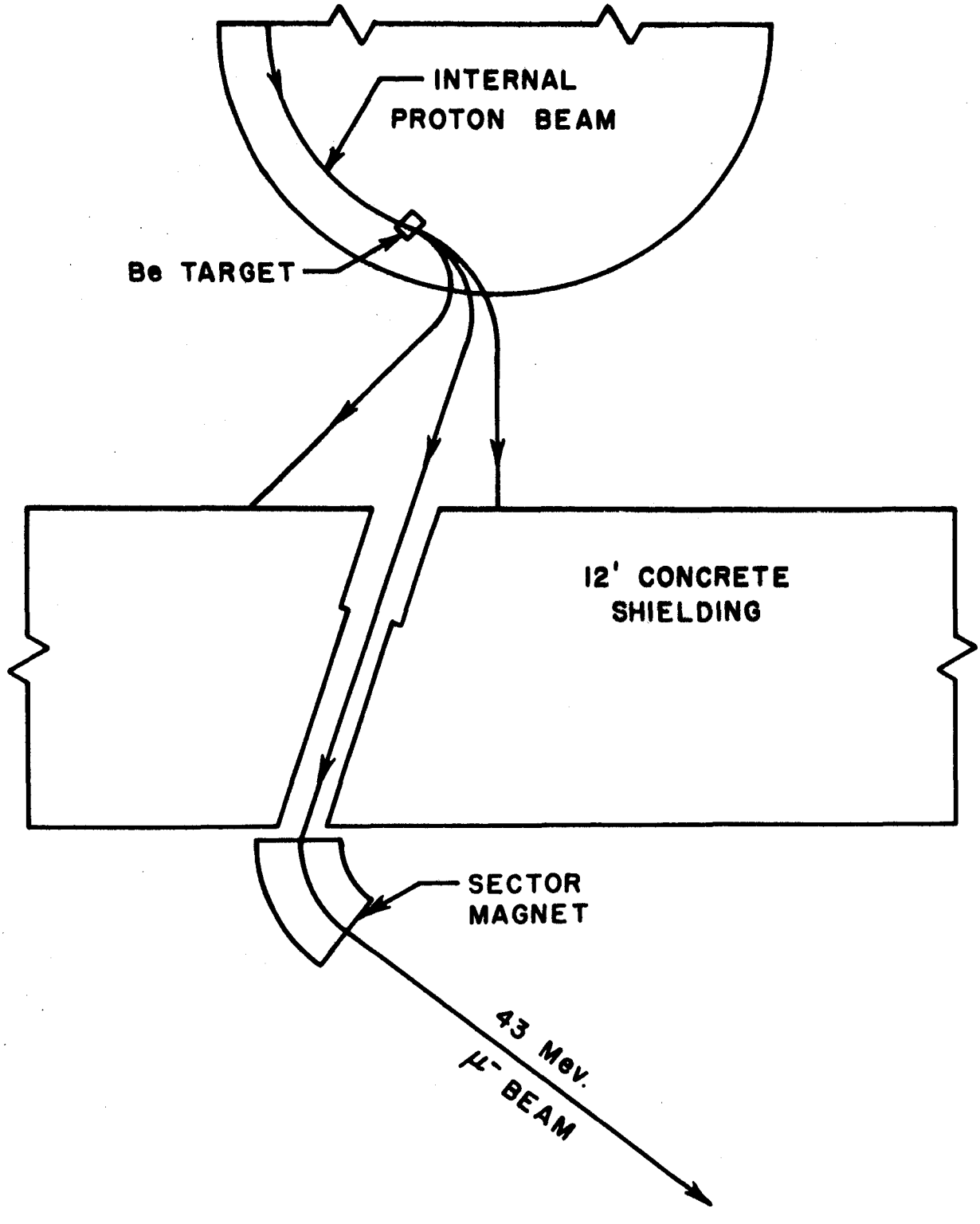


NOT TO SCALE

FIG. 1

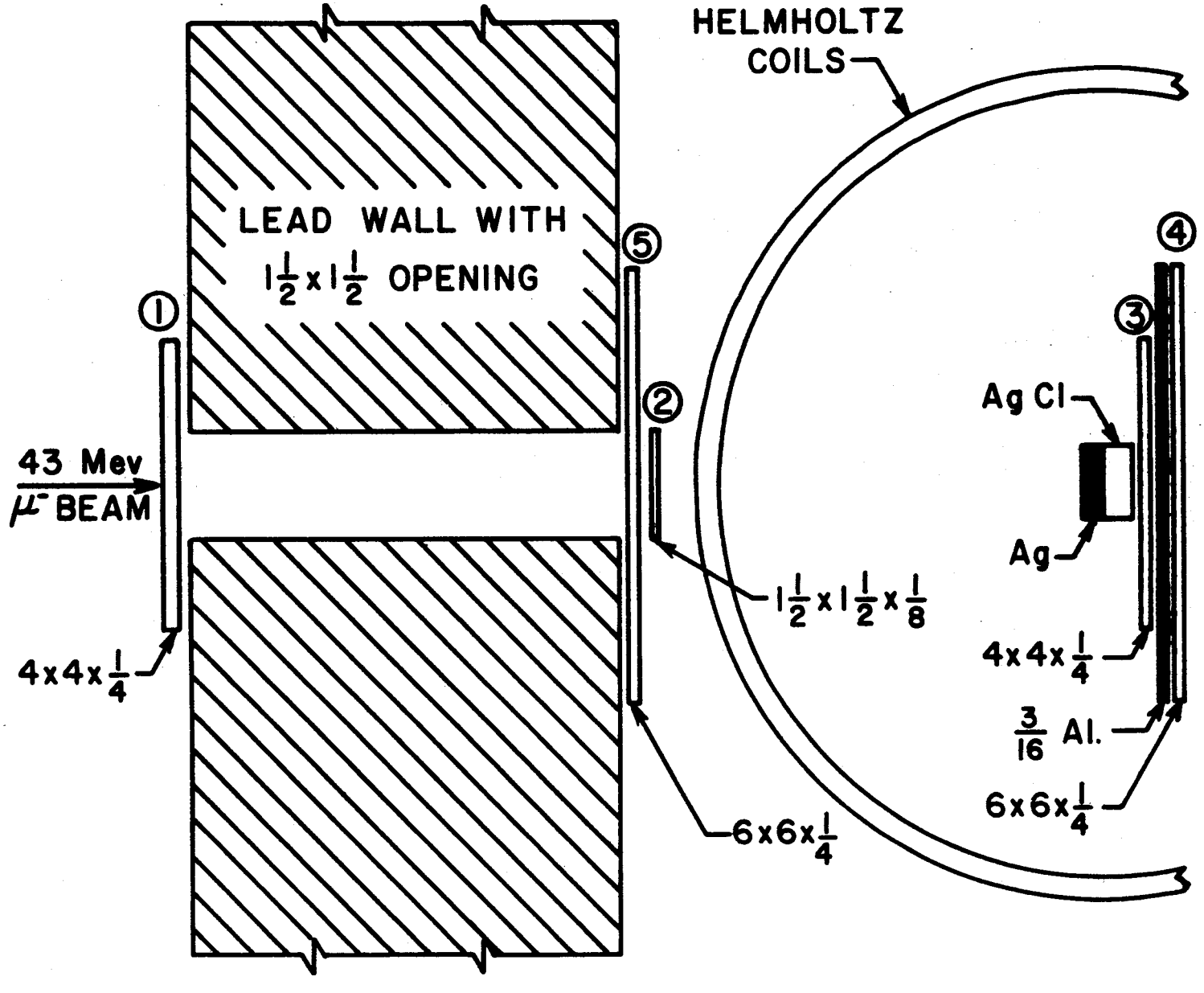
HELMHOLTZ
COILS
LEAD WALL WITH
1½ x 1½ OPENING
①
②
③
④
⑤
43 Mev
μ⁻ BEAM
4x4x¼
1½ x 1½ x ⅛
Ag Cl
Ag
4x4x¼
3/16 Al.
6x6x¼
6x6x¼

FIG. 2

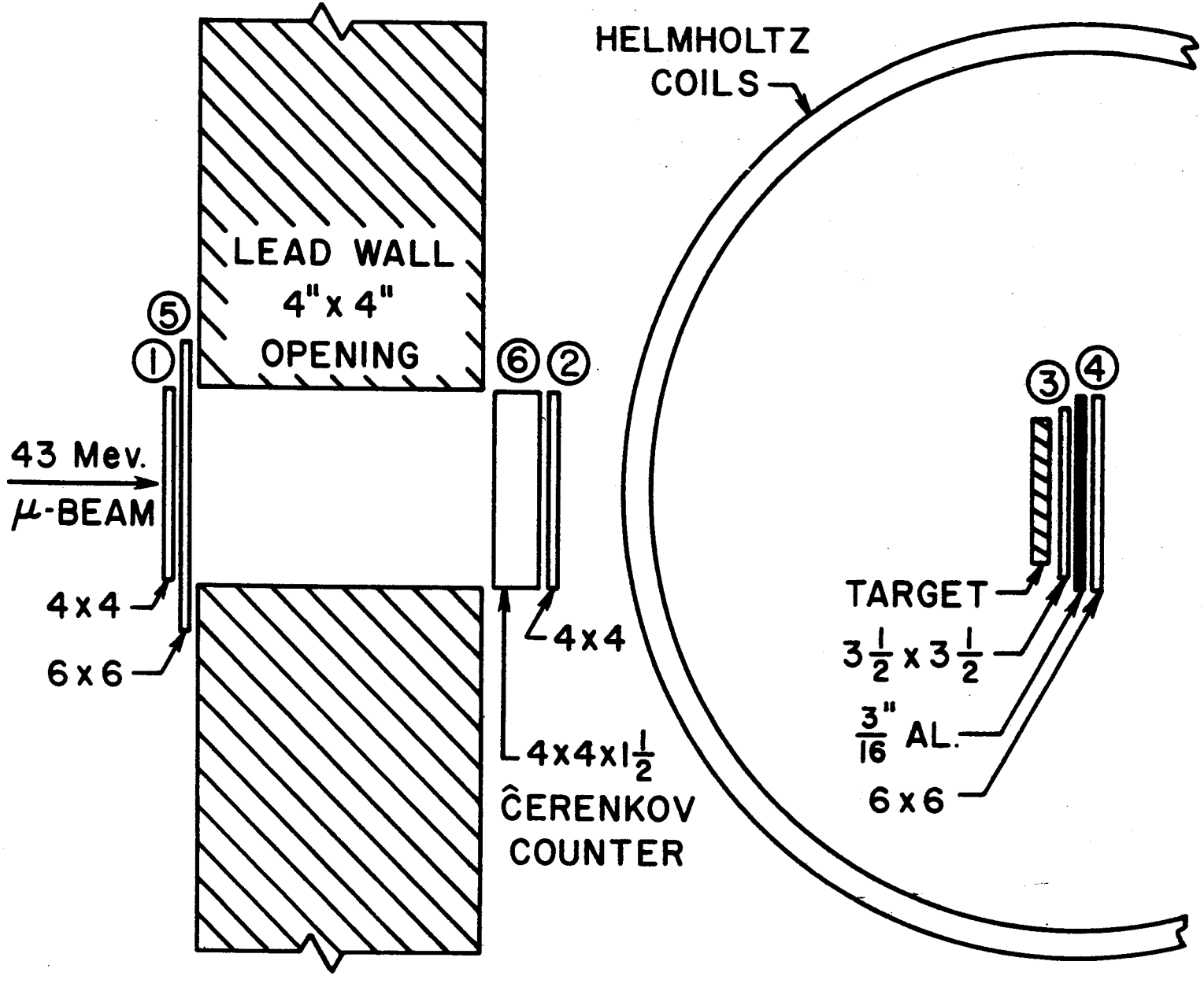
HELMHOLTZ
COILS
LEAD WALL
4" x 4"
OPENING
⑤
①
⑥
②
③
④
43 Mev.
μ-BEAM
4x4
6x6
4x4
4x4x1½
ČERENKOV
COUNTER
TARGET
3½ x 3½
3/16" AL.
6x6

FIG. 3

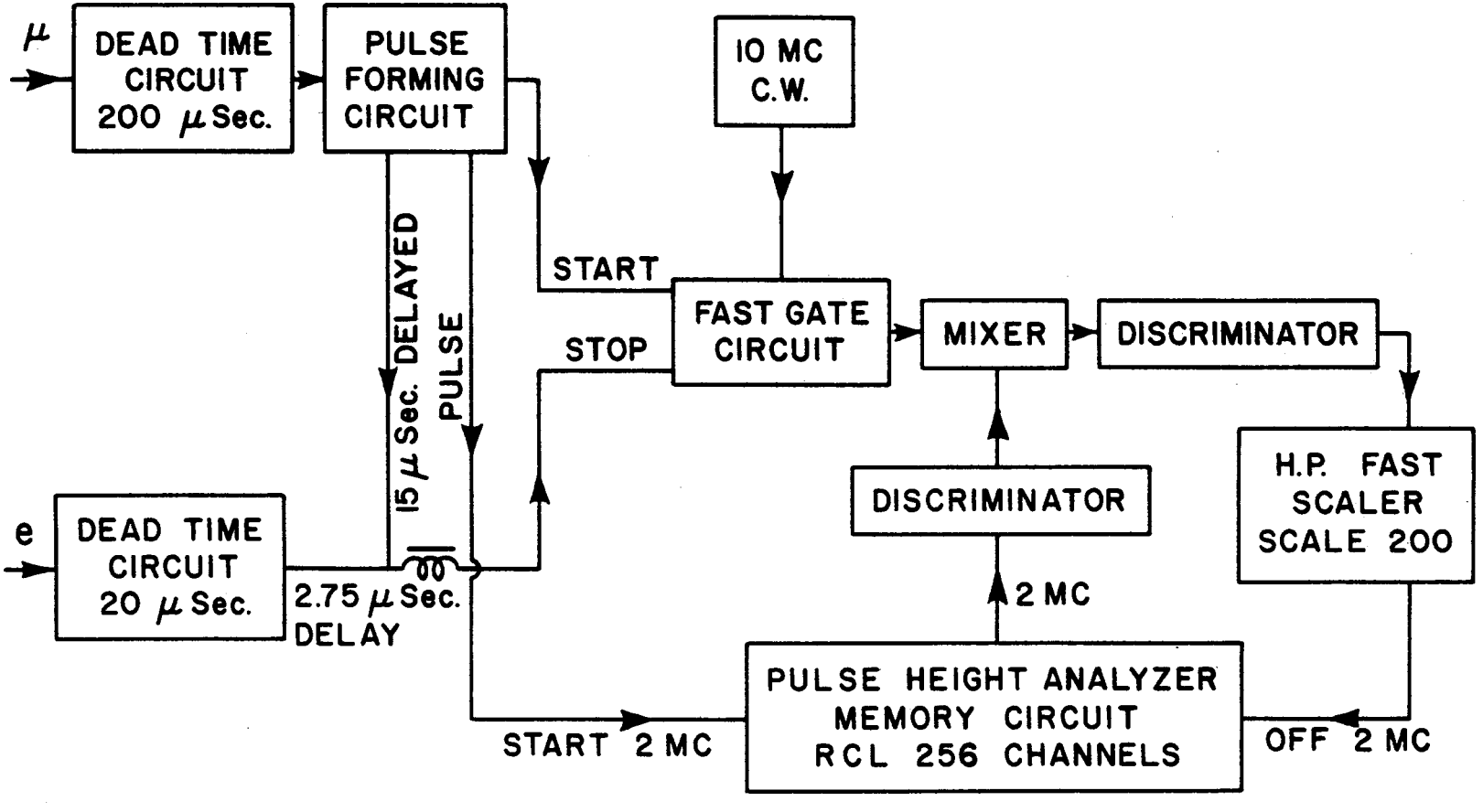
μ
DEAD TIME CIRCUIT 200 μ Sec.
PULSE FORMING CIRCUIT
10 MC C.W.
START
STOP
FAST GATE CIRCUIT
MIXER
DISCRIMINATOR
15 μ Sec. DELAYED PULSE
e
DEAD TIME CIRCUIT 20 μ Sec.
2.75 μ Sec. DELAY
DISCRIMINATOR
H.P. FAST SCALER SCALE 200
2 MC
PULSE HEIGHT ANALYZER MEMORY CIRCUIT RCL 256 CHANNELS
START 2 MC
OFF 2 MC

FIG. 4

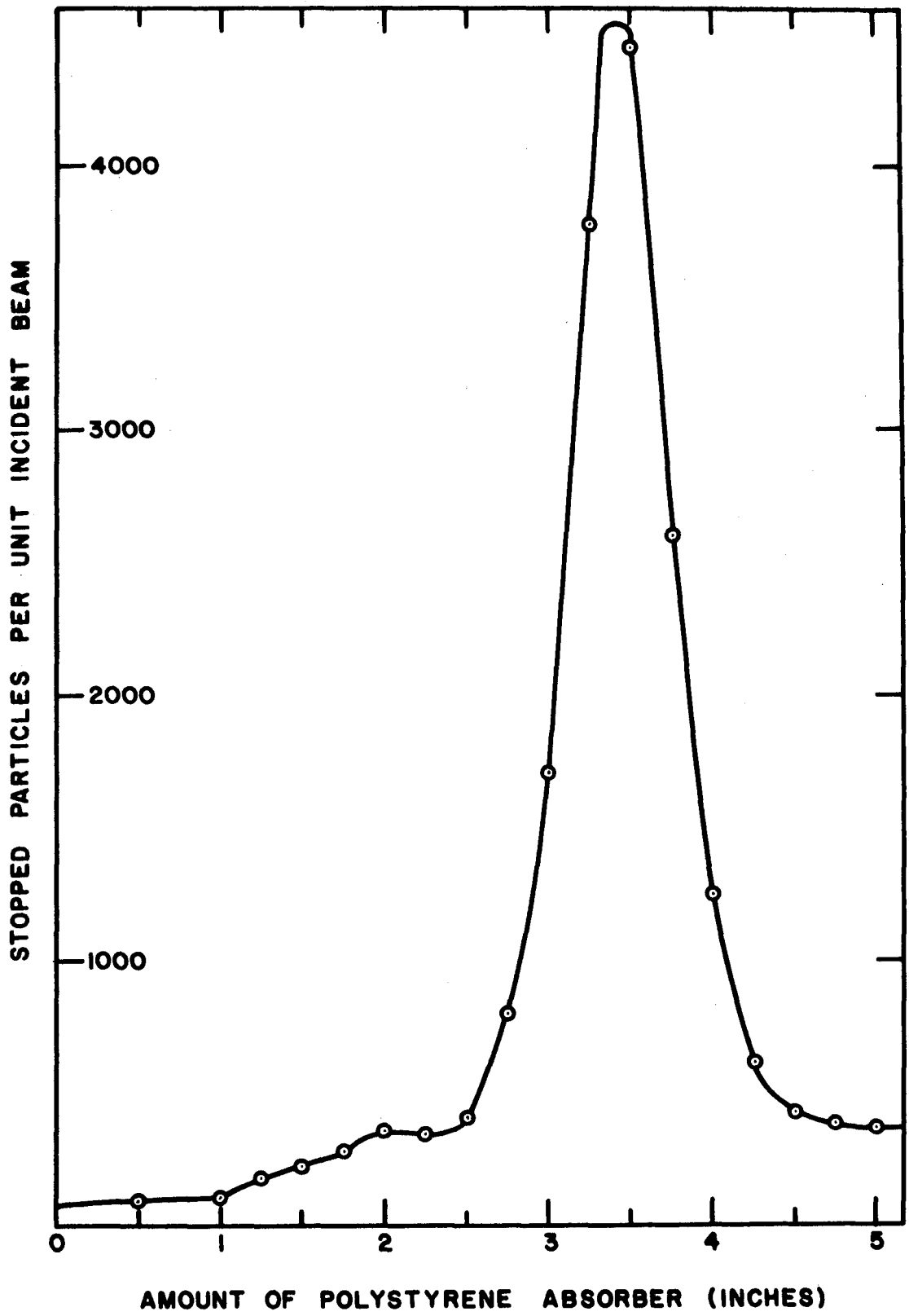
4000
3000
2000
1000
STOPPED PARTICLES PER UNIT INCIDENT BEAM
0
1
2
3
4
5
AMOUNT OF POLYSTYRENE ABSORBER (INCHES)

FIG. 5

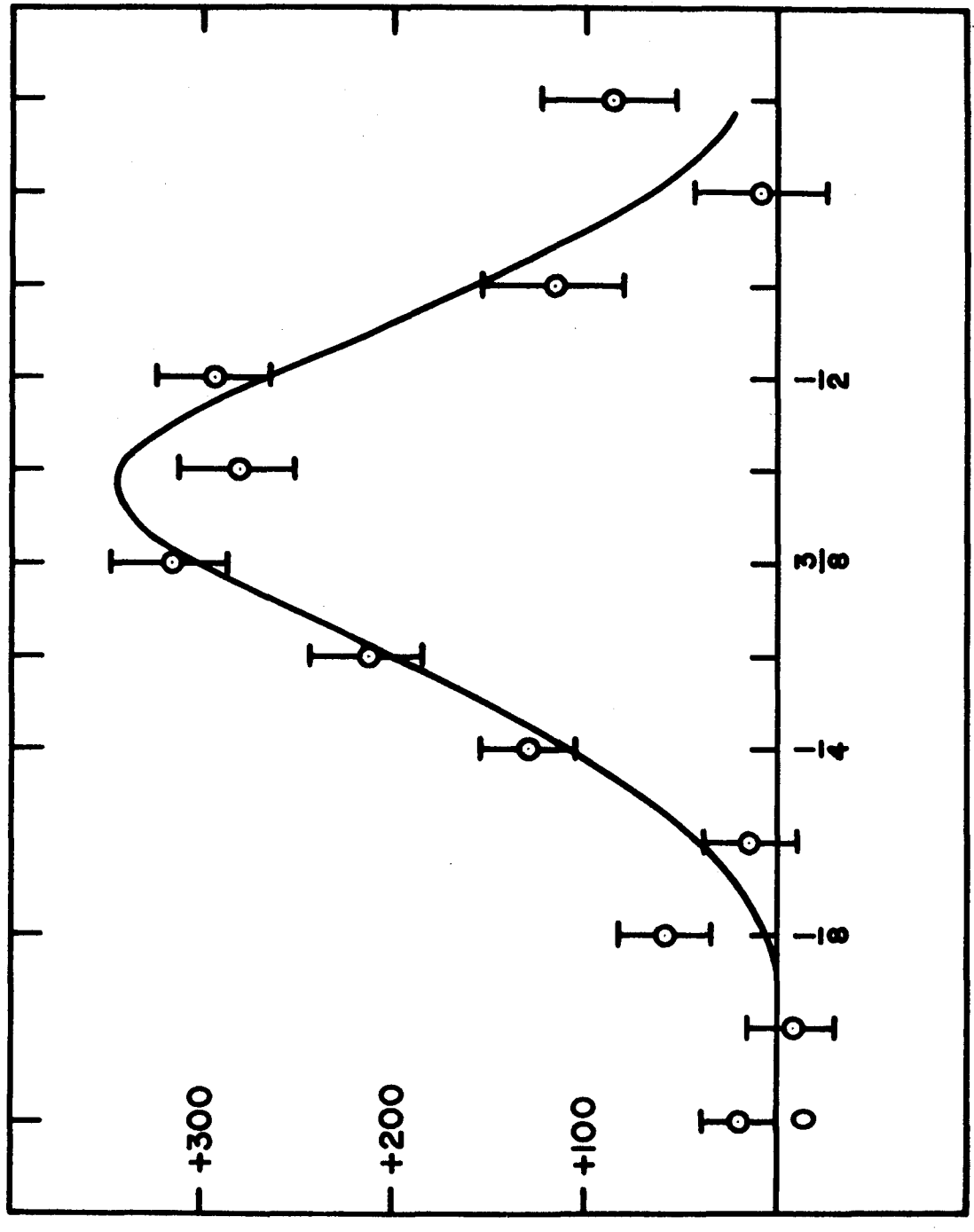
+300
+200
+100
0
1/2
3/8
1/4
1/8
STOPPED MUONS PER UNIT BEAM
AMOUNT OF SILVER ABSORBER IN INCHES

FIG. 6

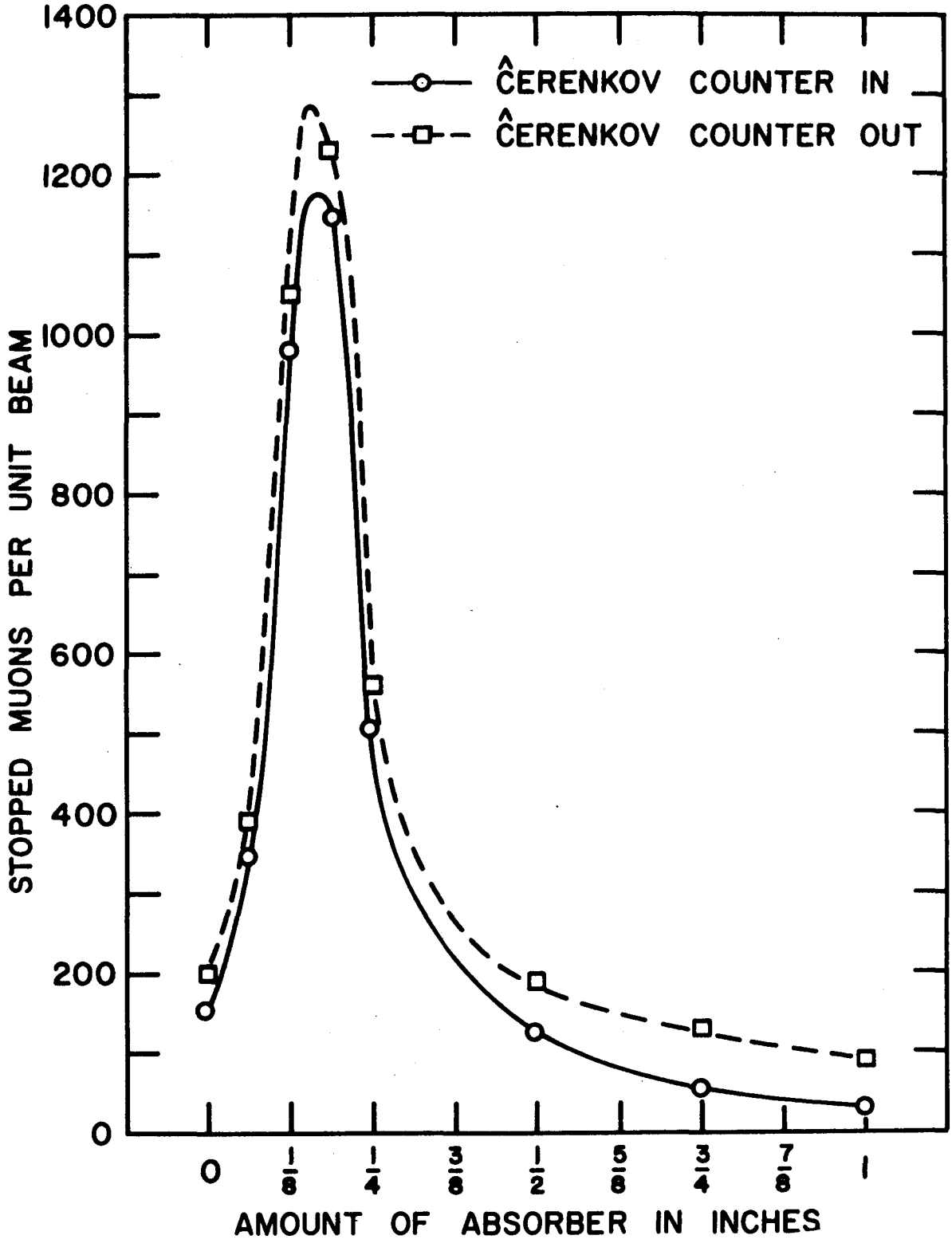
ĈERENKOV COUNTER IN
ĈERENKOV COUNTER OUT
STOPPED MUONS PER UNIT BEAM
1400
1200
1000
800
600
400
200
0
0
1/8
1/4
3/8
1/2
5/8
3/4
7/8
1
AMOUNT OF ABSORBER IN INCHES

FIG. 7

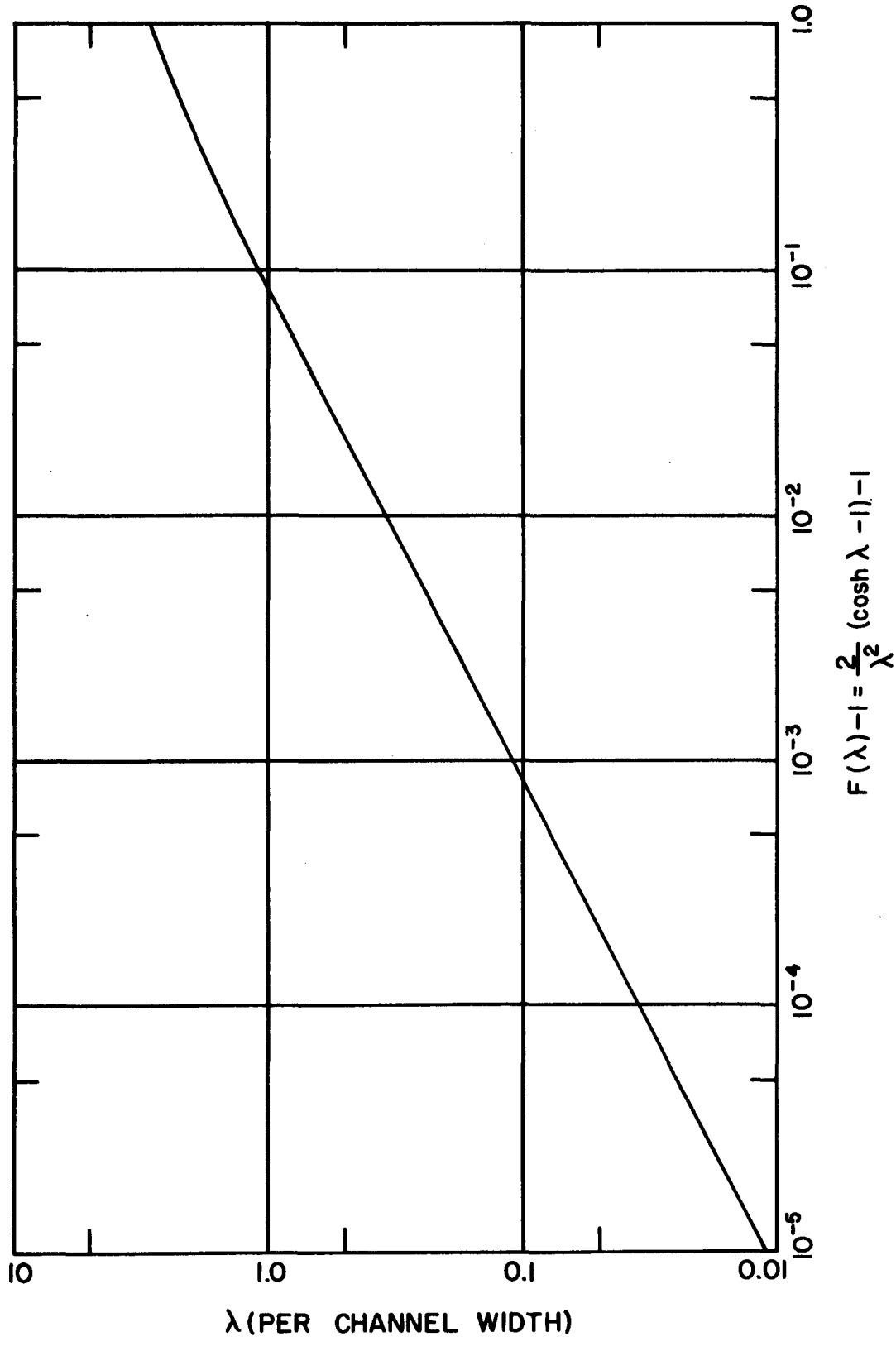
1.0
$10^{-1}$
$10^{-2}$
$10^{-3}$
$10^{-4}$
$10^{-5}$
$F(\lambda)-1=\frac{2}{\lambda^2}(\cosh\lambda-1)-1$
10
1.0
0.1
0.01
λ (PER CHANNEL WIDTH)

FIG. 8

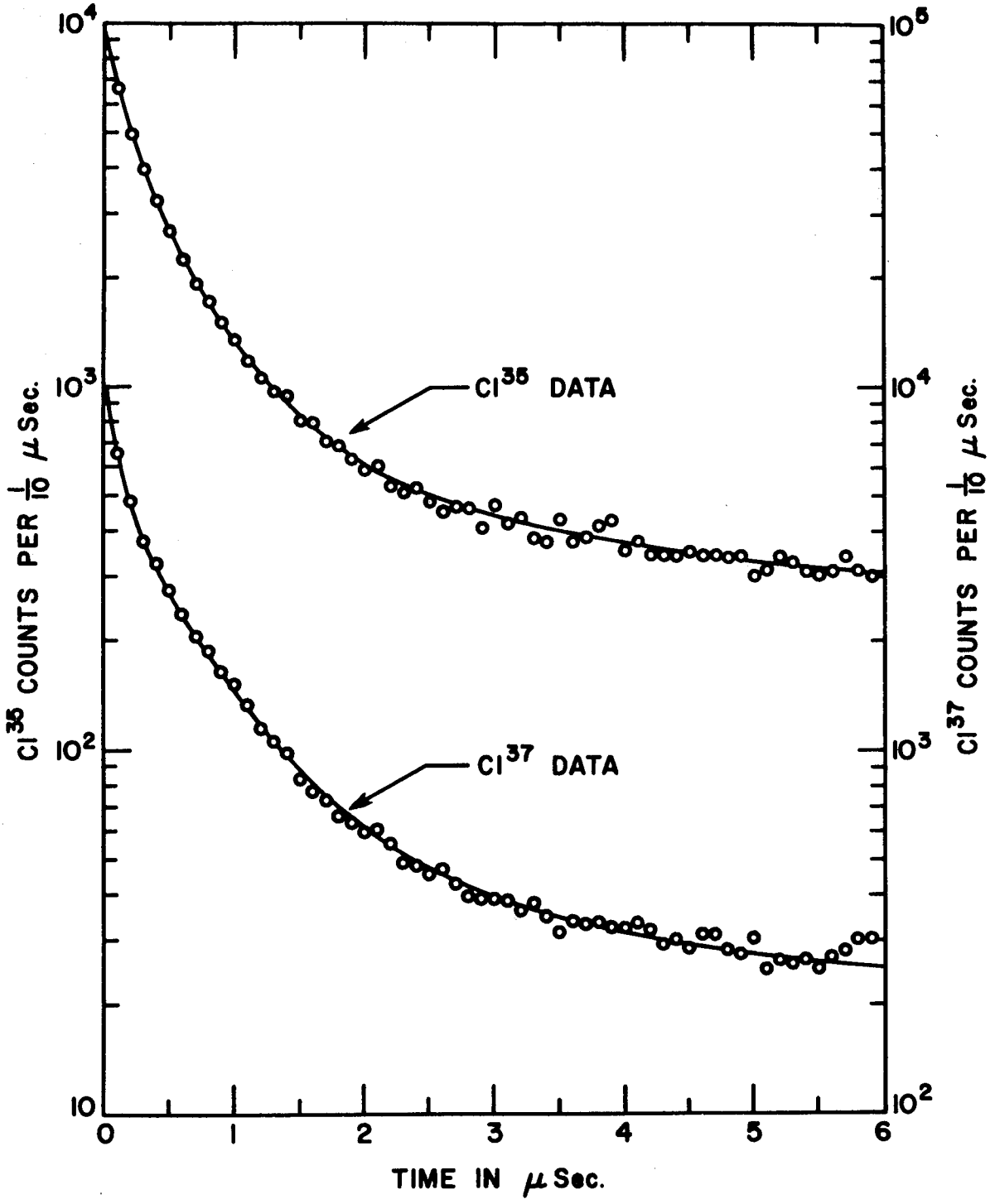
$10^4$
$10^3$
$10^2$
10
$10^5$
$10^4$
$10^3$
$10^2$
$Cl^{35}$ DATA
$Cl^{37}$ DATA
$Cl^{35}$ COUNTS PER $\frac{1}{10}$ $\mu$Sec.
$Cl^{37}$ COUNTS PER $\frac{1}{10}$ $\mu$Sec.
0
1
2
3
4
5
6
TIME IN $\mu$Sec.

FIG. 9

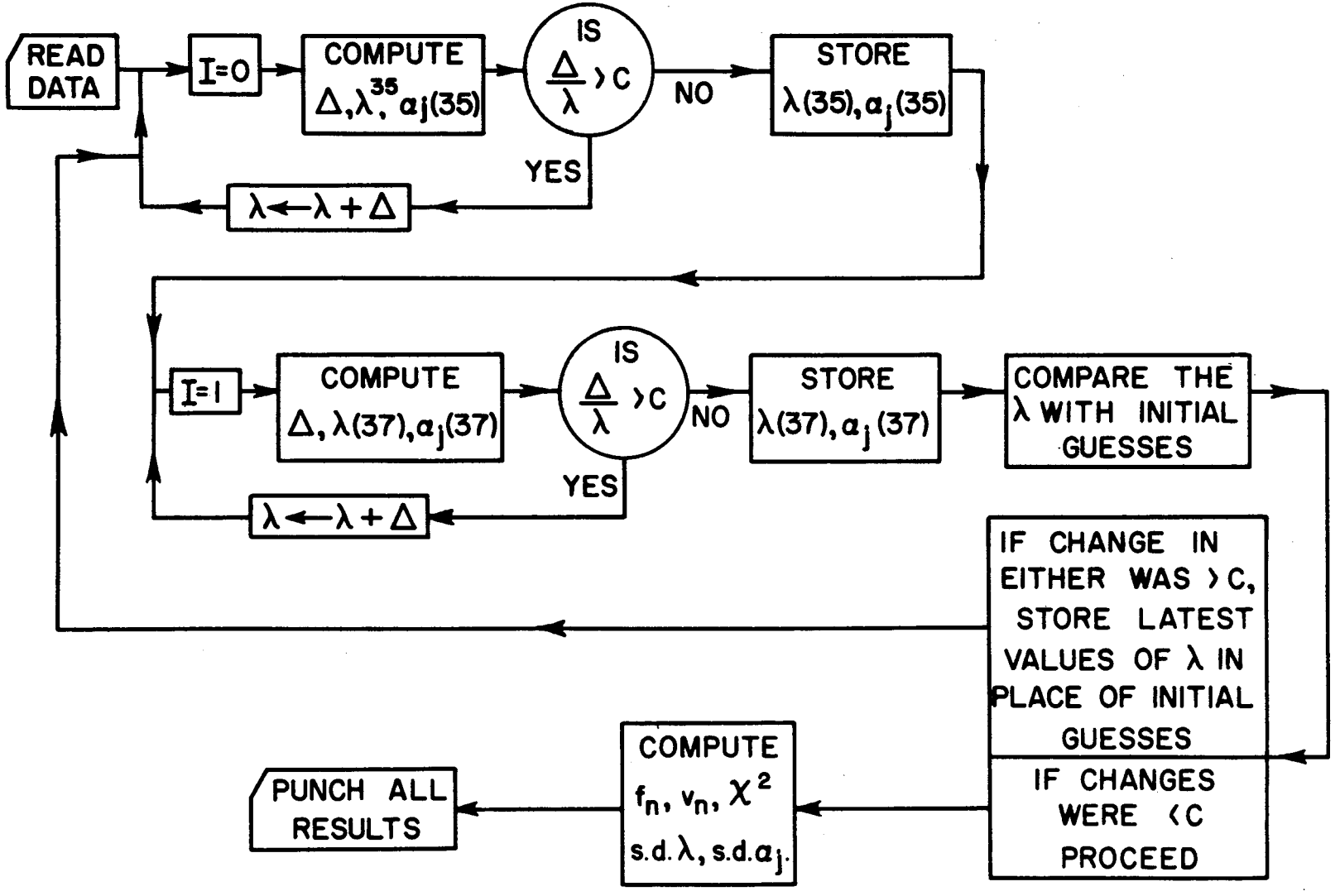
READ DATA
I=0
COMPUTE Δ, λ, $^{35}\alpha_j(35)$
IS $\frac{\Delta}{\lambda} > C$
NO
STORE λ(35), $\alpha_j(35)$
YES
λ ← λ + Δ
I=1
COMPUTE Δ, λ(37), $\alpha_j(37)$
IS $\frac{\Delta}{\lambda} > C$
NO
STORE λ(37), $\alpha_j(37)$
COMPARE THE λ WITH INITIAL GUESSES
YES
λ ← λ + Δ
IF CHANGE IN EITHER WAS > C, STORE LATEST VALUES OF λ IN PLACE OF INITIAL GUESSES
IF CHANGES WERE < C PROCEED
COMPUTE $f_n$, $v_n$, $\chi^2$ s.d.λ, s.d.$\alpha_j$.
PUNCH ALL RESULTS

FIG. 10a

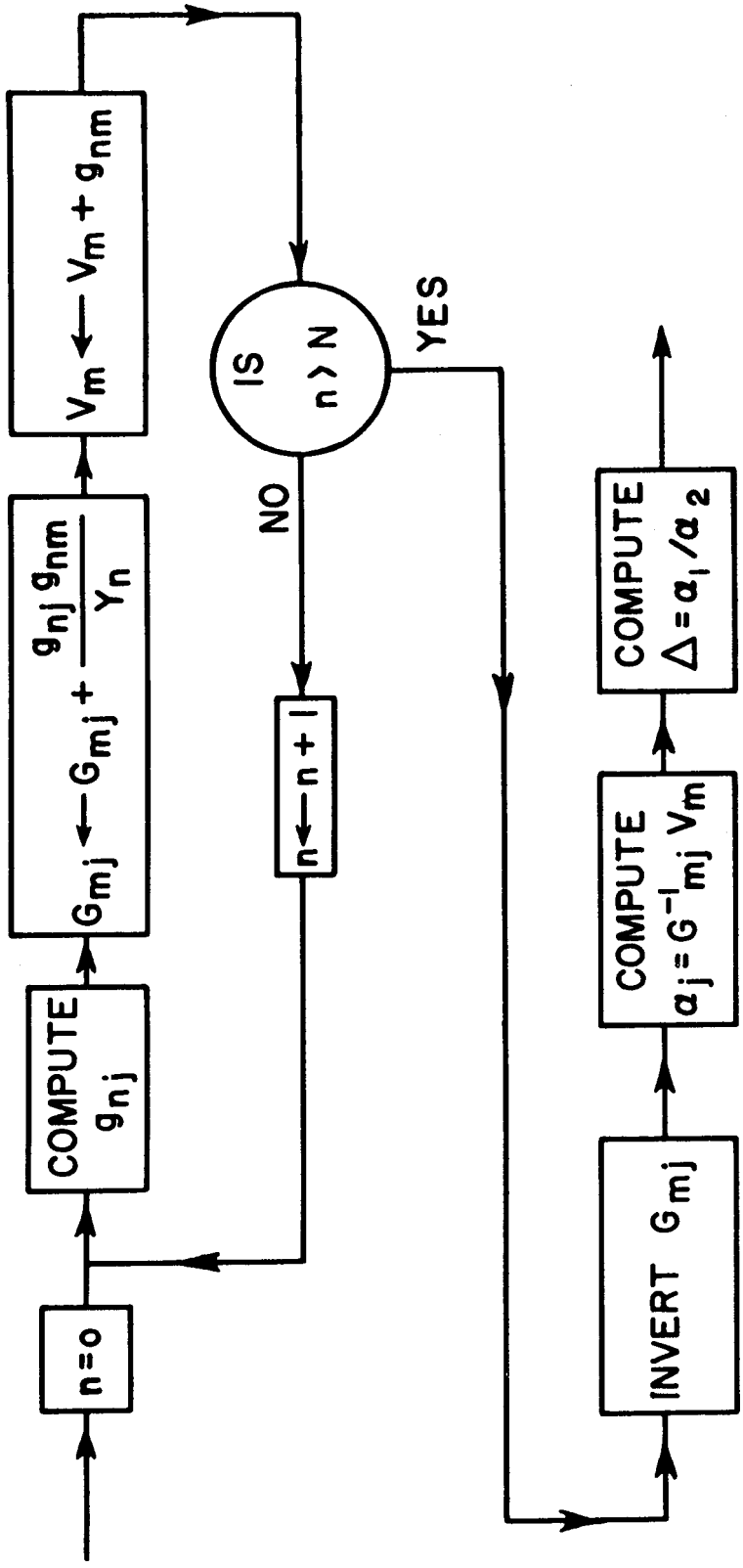
n=0
COMPUTE $g_{nj}$
$G_{mj} \leftarrow G_{mj} + \frac{g_{nj}\, g_{nm}}{Y_n}$
$V_m \leftarrow V_m + g_{nm}$
IS $n > N$
NO
$n \leftarrow n+1$
YES
INVERT $G_{mj}$
COMPUTE $a_j = G^{-1}_{mj}\, V_m$
COMPUTE $\Delta = a_1 / a_2$

FIG. 10b